Cellular and Molecular Life Sciences (2022) 79:162
https://doi.org/10.1007/s00018-022-04182-9

Cellular and Molecular Life Sciences

ORIGINAL ARTICLE

The Alzheimer's gene *SORL1* is a regulator of endosomal traffic and recycling in human neurons

Swati Mishra[1,2] · Allison Knupp[1,2] · Marcell P. Szabo[1,2] · Charles A. Williams[1,2] · Chizuru Kinoshita[1,2] · Dale W. Hailey[1,2] · Yuliang Wang[2,3] · Olav M. Andersen[4] · Jessica E. Young[1,2]

Received: 23 August 2021 / Revised: 24 January 2022 / Accepted: 31 January 2022
© The Author(s) 2022

Abstract

Background Loss of the Sortilin-related receptor 1 (*SORL1*) gene seems to act as a causal event for Alzheimer's disease (AD). Recent studies have established that loss of *SORL1*, as well as mutations in autosomal dominant AD genes *APP* and *PSEN1/2*, pathogenically converge by swelling early endosomes, AD's cytopathological hallmark. Acting together with the retromer trafficking complex, *SORL1* has been shown to regulate the recycling of the amyloid precursor protein (APP) out of the endosome, contributing to endosomal swelling and to APP misprocessing. We hypothesized that *SORL1* plays a broader role in neuronal endosomal recycling and used human induced pluripotent stem cell-derived neurons (hiPSC-Ns) to test this hypothesis. We examined endosomal recycling of three transmembrane proteins linked to AD pathophysiology: APP, the BDNF receptor Tropomyosin-related kinase B (TRKB), and the glutamate receptor subunit AMPA1 (GLUA1).

Methods We used isogenic hiPSCs engineered to have *SORL1* depleted or to have enhanced *SORL1* expression. We differentiated neurons from these cell lines and mapped the trafficking of APP, TRKB and GLUA1 within the endosomal network using confocal microscopy. We also performed cell surface recycling and lysosomal degradation assays to assess the functionality of the endosomal network in both *SORL1*-depleted and -overexpressing neurons. The functional impact of GLUA1 recycling was determined by measuring synaptic activity. Finally, we analyzed alterations in gene expression in *SORL1*-depleted neurons using RNA sequencing.

Results We find that as with APP, endosomal trafficking of GLUA1 and TRKB is impaired by loss of *SORL1*. We show that trafficking of all three cargoes to late endosomes and lysosomes is affected by manipulating SORL1 expression. We also show that depletion of *SORL1* significantly impacts the endosomal recycling pathway for APP and GLUA1 at the level of the recycling endosome and trafficking to the cell surface. This has a functional effect on neuronal activity as shown by multi-electrode array (MEA). Conversely, increased *SORL1* expression enhances endosomal recycling for APP and GLUA1. Our unbiased transcriptomic data further support *SORL1*'s role in endosomal recycling. We observe altered expression networks that regulate cell surface trafficking and neurotrophic signaling in SORL1-depleted neurons.

Conclusion Collectively, and together with other recent observations, these findings suggest that one role for *SORL1* is to contribute to endosomal degradation and recycling pathways in neurons, a conclusion that has both pathogenic and therapeutic implications for Alzheimer's disease.

Keywords Human induced pluripotent stem cells · Neurons · Alzheimer's disease · Endosomal network · *SORL1*

Abbreviations

AD	Alzheimer's disease
SORL1	Sortilin-related receptor 1
SORLA	Sortilin-related receptor with A-type repeats
APP	Amyloid precursor protein
TRKB	Tropomyosin-related kinase B
GLUA1	Glutamate receptor subunit AMPA1
AMPA	α-Amino-3-hydroxy-5-methyl-4-isoxazolepropionic acid
OE	Overexpression
KO	Knockout
WT	Wild type
LAMP1	Lysosome-associated membrane glycoprotein 1
M6PR	Mannose-6-phosphate receptor

Swati Mishra and Allison Knupp contributed equally to this work.

✉ Jessica E. Young
jeyoung@uw.edu

Extended author information available on the last page of the article

Published online: 28 February 2022

GGA	Golgi-localized γ-ear-containing ARF-binding
Rab	Ras-related protein

Background

Alzheimer's disease (AD) is a progressive neurodegenerative disorder and the most common cause of dementia. The underlying contributors to AD pathology encompass several biological pathways, including endosomal function, amyloid precursor protein (APP) processing, immune function, synaptic function, and lipid metabolism [40]. Among these, endosomal dysfunction in neurons is emerging as a potential causal mechanism[84]. Mutations in the amyloid precursor protein (*APP*) and the two presenilins (*PSEN1* and *PSEN2*) lead to early-onset autosomal dominant AD. When these mutations are modeled in human neurons and other systems, they cause endosomal swelling, indicative of traffic jams, a phenotype that is a cytopathological hallmark of AD [9, 12, 44]. Recent genetic studies have identified a fourth gene, the trafficking receptor 'sortilin related receptor 1' (*SORL1*), which, when harboring frame-shift mutations leading to premature stop codons, is described as causal for AD [33, 66, 73]. Interestingly, *SORL1* is also linked to the more common, late-onset form of AD [45, 70] and its expression is lost in sporadic AD brains [4, 21, 59, 89]. When modeled in human neurons, *SORL1* depletion phenocopies *APP* and *PSEN* mutations by causing endosomal swelling [37, 42].

The *SORL1* gene codes for the protein SORLA, an endosomal sorting protein that is also an adaptor molecule for the retromer trafficking complex [25, 70, 83]. Retromer recycles cargo out of the early endosome, either from the endosome to the trans-Golgi network or with greater importance for neurons, back to the cell surface [25, 77]. To date, the best evidence for *SORL1*'s role in retromer-dependent endosomal recycling comes from studies investigating APP trafficking [25, 75, 93]. Our previous work in human neurons demonstrated that *SORL1* depletion retains APP in early endosomes, which may contribute to endosomal swelling by blocking recycling [42].

Retromer-dependent trafficking in neurons, however, also recycles cargo other than APP. For example, retromer is required for the normal recycling of glutamate receptors, a trafficking event that mediates synaptic plasticity and synaptic health, and this dependency occurs independent of retromer's role in APP recycling [61, 88]. Neurotrophin receptors are also trafficked through the endosomal system, in a retromer-dependent manner, and are important for synaptic health [41, 62, 71].

Here, we used human induced pluripotent stem cell-derived neurons (hiPSC-Ns) to test the hypothesis that *SORL1* plays a broader role in neuronal endosomal recycling. We use our previously described *SORL1*-depleted hiPSC lines to generate hiPSC-Ns, which model the loss of *SORL1* expression that occurs in AD [42]. Furthermore, we used previously established cell lines engineered to overexpress *SORL1* two- to threefold over wild-type levels [96] to test the effects of enhanced *SORL1* expression in hiPSC-Ns on these trafficking pathways. Importantly, all cell lines are isogenic. We map the trafficking effects these manipulations have on three specific proteins known to sort through the endosome recycling pathway: APP, the GLUA1 subunit of the AMPA receptor, and neurotrophin receptor TRKB, all of which are implicated in AD [18, 19, 26, 53, 91, 95].

Finally, we performed RNA sequencing on the *SORL1*-depleted cell lines to explore an unbiased transcriptomics analysis induced by *SORL1* depletion. The results generally confirmed our hypothesis, showing that one role for *SORL1* is to contribute to endosomal degradation and recycling pathways in neurons, a conclusion that has both pathogenic and therapeutic implications.

Methods

Cell lines

Cell lines generated by CRISPR/Cas9 gene-editing technology

The generation of the cell lines used in this paper is described in our previously published work [42] and consists of four clones: two wild-type clones, designated clone A6 and clone A7, and two *SORL1*KO clones, designated clone E1 and clone E4. Cell lines were generated from our previously published and characterized CV background human induced pluripotent stem cell line [96]. This cell line is male and has a APOE ε3/ε4 genotype [47]. All four clones were shown to have normal karyotypes and are routinely tested for mycoplasma (MycoAlert). The clones used in the experiments in this work are listed in the figure legends.

CRISPR/Cas9 gRNA, ssODN, and primer sequences: gRNA: ATTGAACGACATGAACCCTC ssODN: GGGAATTGATCCCTATGACAAACCAAATACCATCTACATTGAACGACATGAACCCTCTGGCTACTCCACGTCTTCCGA AGTACAGATTTCTTCCAGTCCCGGGAAAACCAGGAAG, Forward primer: ctctatcctgagtcaaggagtaac, Reverse primer: ccttccaattcctgtgtatgc, PCR amplifies 458 bp sequence. These sequences have been previously published in [42].

SORL1 overexpression cell lines: isogenic cell lines with overexpression of SORL1 were generated as previously described [96]. These lines are generated from the CV parental line, the same parental line as the *SORL1*KO cell lines were made from. Briefly, stable integration of SORL1 cDNA into the genome was achieved using piggybac transposon system (Systems Biosciences). Vector alone (WT) or vector with SORL1 cDNA (*SORL1*OE) constructs were introduced into iPSCs by electroporation and stable cell lines were selected with puromycin (2 µg/ml) treatment. We obtained one SORL1OE stable cell line and one vector alone stable cell line. For all overexpression experiments, *SORL1*OE cells were compared to the vector alone controls.

hiPSC neuronal differentiation

hiPSCs were differentiated to neurons using dual-SMAD inhibition [10, 79]. Briefly, hiPSCs were plated on Matrigel coated 6-well plates at a density of 3.5 million cells per well and fed with Basal Neural Maintenance Media (1:1 DMEM/F12 + glutamine media/neurobasal media, 0.5% N2 supplement, 1% B27 supplement, 0.5% GlutaMax, 0.5% insulin-transferrin-selenium, 0.5% NEAA, 0.2% β-mercaptoethanol; Gibco, Waltham, MA) + 10 mM SB-431542 + 0.5 mM LDN-193189 (Biogems, Westlake Village, CA). Cells were fed daily for 7 days. On day 8, cells were incubated with Versene, gently dissociated using cell scrapers, and passaged at a ratio of 1:3. On day 9, media was switched to Basal Neural Maintenance Media and fed daily. On day 13, media were switched to Basal Neural Maintenance Media with 20 ng/ml FGF (R&D Systems, Minneapolis, MN) and fed daily. On day 16, cells were passaged again at a ratio of 1:3. Cells were fed until approximately day 23. At this time, cells were FACS sorted to obtain the CD184/CD24-positive and CD44/CD271-negative neural precursor cell (NPC) population. Following sorting, NPCs were expanded for neural differentiation. For cortical neuronal differentiation, NPCs were plated out in 10 cm cell culture dishes at a density of 6 million cells/10 cm plate. After 24 h, cells were switched to Neural Differentiation media (DMEM-F12 + glutamine, 0.5% N2 supplement, 1% B27 supplement, 0.5% GlutaMax) + 0.02 µg/ml brain-derived neurotrophic factor (PeproTech, Rocky Hill, NJ) + 0.02 µg/ml glial-cell-derived neurotrophic factor (PeproTech) + 0.5 mM dbcAMP (Sigma Aldrich, St Louis, MO). Media was refreshed twice a week for 3 weeks. After 3 weeks, neurons were selected for CD184/CD44/CD271-negative population by MACS sorting and plated for experiments. The data presented in this study represent 2–3 neuronal differentiations.

Purification of neurons

Following 3 weeks of differentiation, neurons were dissociated with accutase and resuspended in Magnet Activated Cell Sorting (MACS) buffer (PBS + 0.5% bovine serum albumin [Sigma Aldrich, St Louis, MO] + 2 mM ethylenediaminetetraacetic acid [Thermo Fisher Scientific, Waltham, MA]). Following a modification of [97], cells were incubated with PE-conjugated mouse anti-Human CD44 and mouse anti-Human CD184 antibodies (BD Biosciences, San Jose, CA) at a concentration of 5 µl/10 million cells. Following antibody incubation, cells were washed with MACS buffer and incubated with anti-PE magnetic beads (BD Biosciences, San Jose, CA) at a concentration of 25 µl/10 million cells. Bead-antibody complexes were pulled down using a rare-earth magnet, supernatants were selected, washed, and plated at an appropriate density.

DQ Red BSA assay for visualization of lysosomal degradation

Lysosomal proteolytic degradation was evaluated using DQ Red BSA (#D-12051; Thermo Fisher Scientific), a fluorogenic substrate for lysosomal proteases, that generates fluorescence only when enzymatically cleaved in intracellular lysosomal compartments. hiPSC-derived neurons were seeded at a density of 400,000 cells/well of a Matrigel coated 48-well plate. After 24 h, cells were washed once with DPBS, treated with complete media containing either 10 µg/ml DQ Red BSA or vehicle (PBS) and incubated for 6 h or 24 h [16, 72, 90] at 37 °C in a 5% CO_2 incubator as described in [54]. At the end of 6 or 24 h, cells were washed with PBS, fixed with 4% PFA and immunocytochemistry was performed as described in "Methods". Cells were imaged using a Leica SP8 confocal microscope and all image processing was completed with ImageJ software. Cell bodies were identified by MAP2 labeling, and fluorescence intensity of DQ Red BSA was measured in regions of the images containing the MAP2 label.

Immunocytochemistry

For immunocytochemistry, cells were fixed with 4% PFA for 20 min. Fixed cells were washed three times with PBST (PBS with 0.05% tween 20), permeabilized with Triton X-100 in PBS for 15 min, washed twice again with PBST, blocked with 5% BSA in PBS at room temperature for 1 h and incubated with appropriate primary antibodies overnight at 4 °C. The next day, cells were incubated with appropriate secondary antibodies and 1 µg/ml DAPI for 1 h at RT, washed three times with PBST and mounted on glass slides with Prolong Gold Antifade mountant (#P36930; Thermo Fisher Scientific).

Colocalization analysis

To investigate colocalization with endo-lysosomal compartments, hiPSC-derived neurons were labeled with markers specific for each intracellular compartment (EEA1 for early endosomes, Rab7 for late endosomes, LAMP1 for lysosomes and Rab11 for recycling endosomes) using immunocytochemistry. A minimum of 10 fields of confocal z-stack images were captured under blinded conditions using a Yokogawa W1 spinning disk confocal microscope (Nikon) and a 100X plan apochromat oil immersion objective. Median filtering was used to remove noise from images and Otsu thresholding was applied to all images. Colocalization was quantified using the JACOP plugin [7] in Image J software [74] and presented as Mander's correlation coefficient [23, 51]. For all imaging experiments, the data were analyzed in a blinded manner.

Cell Surface Staining: cell surface expression of GLUA1 and APP was determined using immunocytochemistry and confocal microscopy. To label proteins at the cell surface, cells were fixed with 4% PFA, washed and treated with primary and secondary antibodies as described in "Immunocytochemistry" section of "Methods". Permeabilization with 0.1% Triton X-100 was not performed for this experiment. To label total protein levels, cells were fixed with 4% PFA, washed, permeabilized with 0.1% Triton X-100 and treated with primary and secondary antibodies as described in "Immunocytochemistry" section of "Methods". Analysis of fluorescence intensity was done using Image J software. Cell surface expression was represented as ratio of fluorescence intensity measured under non-permeabilized conditions and fluorescence intensity measured under permeabilized conditions. For all imaging experiments, the data were analyzed in a blinded manner.

Multielectrode (MEA) assay

hiPSC-derived neural progenitor cells were differentiated into neurons, and neurons were purified as previously described in "Methods". Purified neurons were mixed with unpurified neurons in a ratio of 5:1, and this mixture was plated onto a Matrigel coated 48-well MEA plate (Axion Biosystems; # M768-tMEA-48 W) at a cell density of 8000 cells/µl (total number of cells/well = 50,000). MEA-plated neurons were initially cultured in neural differentiation media. Media was gradually switched to BrainPhys media (Stem cell technologies; # 05790) by replacing half of a well's media twice a week. BrainPhys media was supplemented with B27, N2, BDNF, GDNF, and dbcAMP.

Multielectrode (MEA) analysis

Electrical signals from neurons in the MEA plates were recorded twice a week using Axion Biosystems Maestro Pro system. Signals were recorded at a sampling frequency of 12.5 kHz with a 3 kHz Kaiser Window low-pass filter and 200 Hz high-pass filter. Spikes were detected using Axion Axis Navigator recording software with the adaptive threshold method. Recordings were analyzed using the Axion Neural Metric Tool. Firing rate data were limited to active electrodes that detected a minimum of five spikes a minute. Firing rate data from all active electrodes in a well were averaged for plotting and statistical testing.

Antibodies

The following primary antibodies were used: Early endosome antigen 1 (EEA1) at 1:500 (#610456; BD Biosciences); amyloid precursor protein (APP) at 1:500 (#ab32136; Abcam); microtubule-associated protein 2 (MAP2) at 1:1000 (ab92434; Abcam); Ras-related protein Rab-7a (Rab7) at 1:1000 (ab50533; Abcam); Ras-related protein Rab-11 (Rab11) at 1:250 (#610656; BD Biosciences); Lysosome-associated membrane protein-1 (LAMP1) at 1:250 (#sc 2011; Santa Cruz); Tropomyosin receptor kinase B (TRKB; # ab18987; abcam) at 1:1000, GLUA1(# MAB2263; Millipore sigma) at 1:500 and VPS35 (Abcam; #ab97545) at 1:500. DAPI was used at a final concentration of 0.1 µg/ml (Alfa Aesar).

Transferrin recycling assay

To measure recycling pathway function, we utilized transferrin recycling assay as previously described [68]. Purified neurons were seeded at 400,000 cells/well of a 24-well plate containing Matrigel coated 12 mm glass coverslip/well. After 5 DIV, cells were washed once with DMEM-F12 medium and incubated with starving medium (DMEM-F12 medium + 25 mM HEPES + 0.5% BSA) for 30 min at 37 °C in a 5% CO_2 incubator to remove any residual transferrin. Thereafter, cells were pulsed with either 100 µg/ml transferrin from human serum conjugated with Alexa Fluor™ 647(#T23366; Thermo Fisher Scientific) or vehicle (PBS) in 'starving medium'. At the end of 10 min, cells were washed twice with ice-cold PBS to remove any external transferrin and stop internalization of transferrin and washed once with acid stripping buffer (25 mM citric acid + 24.5 mM sodium citrate + 280 mM sucrose + 0.01 mM Deferoxamine) to remove any membrane bound transferrin. Next, cells were either fixed in 4% PFA or 'Chase medium' (DMEM-F12 + 50 µM Deferoxamine + 20 mM HEPES + 500 µg/ml Holo-transferrin) was added for different time points. Immunocytochemistry was done using MAP2 antibody to label neurons, confocal images were captured using Leica SP8 confocal microscope under blinded conditions. Fluorescence intensity of transferrin was measured using ImageJ software. Recycling function was presented as transferrin fluorescence intensity as a percentage of the fluorescence intensity measured at time zero.

Measurement of lysosome and recycling endosome size

Immunocytochemistry using antibodies for LAMP1 and MAP2 or RAB11 and MAP2 was performed as described above. Using a Leica SP8 confocal microscope with an apochromatic 63X oil immersion lens, z-stack images were obtained under blinded conditions. For the LAMP1 analysis, 17–34 fields were analyzed for a total of 45–76 cells analyzed. For the RAB11 analysis, 15–30 fields were analyzed for a total of 59–124 cells analyzed. Vesicle size measurements were performed using Cell Profiler software as previously described [42, 57]. Briefly, the vesicle channel was masked using the MAP2 channel and automated segmentation algorithms were used to identify individual puncta. The pixel area of each puncta was measured and is presented as mean area of all puncta per field.

Statistical analysis

For all imaging experiments, data were collected and analyzed in a blinded manner. Data were assessed for significance using parametric two-tailed unpaired Student's *t*-tests or two-way ANOVA tests. Data are represented as mean ± standard deviation to show the spread of the data. Significance was defined as a value of $p \leq 0.05$. All statistical analyses were completed using GraphPad Prism software. Statistical details of individual experiments, including biological and technical replicate information, can be found in the figure legends. All the raw statistical data for the experiments in this paper, including means, difference between the means ± SEM, and 95% confidence intervals are presented in Supplemental Table 1.

RNA-sequencing analysis

RNA extraction

RNA was collected from 3 separate differentiations including a combination of two WT clones and two *SORL1*KO clones. Each sample includes 2–3 technical replicates. RNA was collected from 2 million purified neurons for each sample. Purification of total RNA was completed using the PureLink RNA Mini Kit (Thermo Fisher 12183018A). Assessment of purified RNA was completed using a NanoDrop. Final RNA quantification was completed using the Quant-iT RNA assay (Invitrogen) and RNA integrity analysis was completed using a fragment analyzer (Advanced Analytical).

Library preparation and sequencing

Library preparation was completed using the TruSeq Stranded mRNA kit (Illumina RS-122–2103) per manufacturer instructions. Sequencing was performed on a NovaSeq 6000 instrument.

Data analysis

Raw reads were aligned to GRCh38 with reference transcriptome GENCODE release 29 using STAR v2.6.1d [20]. Gene-level expression quantification is generated by RSEM v1.3.1 [48]. Genes with fewer than 20 normalized reads across all samples were omitted from further analysis. We did observe variation in the transcriptome based on differentiation (Supplemental Figure 3A); however, this was corrected for using the sva package [46].

To identify differentially expressed genes (DEGs), we used DESeq [3]. Briefly, we fit two models: a null model where gene expression only depends on batch effects (i.e., differentiation), and an alternative model where gene expression depends on both genotype (*SORL1*KO vs. WT) and batch effects. Chi-squared tests were performed to compare both fits, and we declare a gene as differentially expressed only when the alternative model fits the expression data better. DEGs are defined as genes with false discovery rate less than 0.05 and fold change greater than 1.5. The top gene ontology package [2] and the SynGO synaptic gene ontology annotations [43] were used to identify GO terms that were enriched. GO terms were tested according to the Fisher's exact test. Finally, we mapped DEGs onto receptor–ligand interaction diagrams generated by Ramilowski et al. [67] using the igraph plugin [13]. To compare the amount of downregulated vs. upregulated genes, we used a 2-sample test for equality of proportions with continuity correction in R.

Results

SORL1 depletion increases neuronal cargo localization in early endosomes

Using CRISPR/Cas9 genome-editing techniques, we previously generated hiPSC-derived neurons (hiPSC-Ns) deficient in *SORL1* expression due to indels introduced in exon 6. We demonstrated that loss of *SORL1* expression in these neurons leads to enlarged early endosomes and an increased localization of APP within early endosomes, indicative of endosomal traffic jams [42]. We utilized these same cell lines (hereafter referred to as *SORL1*KO and their guide-matched isogenic wild-type clones referred to as WT) to examine localization of the BDNF receptor TRKB and the GLUA1 subunit of the neuronal AMPA receptor. TRKB has been shown to bind to SORLA and this interaction mediates trafficking of TRKB to synaptic plasma membranes [71]. GLUA1 is trafficked via the retromer complex, of which SORLA is an adaptor protein [25, 88] and both of these cargoes are important in maintaining healthy neuronal function. Since we previously observed an increase in APP localization in early endosomes, resulting in a decrease in localization in downstream vesicles such as Ras-related protein (Rab)7 + late endosomes with *SORL1* depletion [42], we performed an immunocytochemical analysis of both TRKB and GLUA1 localization with the early endosome marker EEA1. Similar to our previous observations for APP, we documented significantly increased localization of both TRKB (Fig. 1A) and GLUA1 (Fig. 1B) in early endosomes in *SORL1*KO neurons as compared to isogenic WT control neurons. Accumulation of neuronal cargo in early endosomes is indicative of endosomal traffic jams, which are thought to impact the transit of cellular cargo through other arms of the endo-lysosomal network. Due to SORLA's role as an adaptor protein for the retromer complex, we also examined whether *SORL1* depletion led to changes in retromer subunit localization. We observed that VPS35, a core subunit of the retromer cargo recognition complex is also mis-localized to early endosomes in the absence of SORLA activity, similar to what we observed for APP, TRKB, and GLUR1 (Supplemental Figure 1).

Modulating *SORL1* expression impacts cargo trafficking throughout the endo-lysosomal system

The early endosome serves as a hub in which internalized cargo can be retrogradely transported to the trans-Golgi, recycled back to the cell surface or degraded as endosomes mature into late endosomes and lysosomes [56]. We have previously observed that APP localization within the trans-Golgi network was decreased in *SORL1*KO neurons [42]. Here, we tested whether trafficking to the degradative arm of the endo-lysosomal network was affected in our *SORL1*KO neurons. Trafficking of substrates out of the early endosome to late endosomes and, subsequently, lysosomes is important for protein degradation and SORLA has been previously implicated in promoting Aβ degradation via lysosomes [8]. We treated *SORL1*-deficient neurons with DQ Red BSA, a proteolysis sensitive fluorogenic substrate that generates fluorescence only when enzymatically cleaved in intracellular lysosomal compartments. Since substrate degradation primarily occurs in lysosomes, altered fluorescence intensity of this reagent is a readout of altered lysosomal degradation [54]. We treated neurons with DQ Red BSA for 6 and 24 h and analyzed fluorescence intensity using confocal microscopy. Consistent with loss of *SORL1* leading to endosomal traffic jams, we observed a significant reduction of DQ Red BSA fluorescence intensity at both time points in *SORL1*KO neurons compared to isogenic WT controls (Fig. 2A). We next performed immunocytochemical staining to quantify the colocalization of our selected neuronal cargo with Rab7, a marker of late endosomes, and LAMP1 (Lysosomal Associated Membrane Protein 1), a lysosome marker. We show a

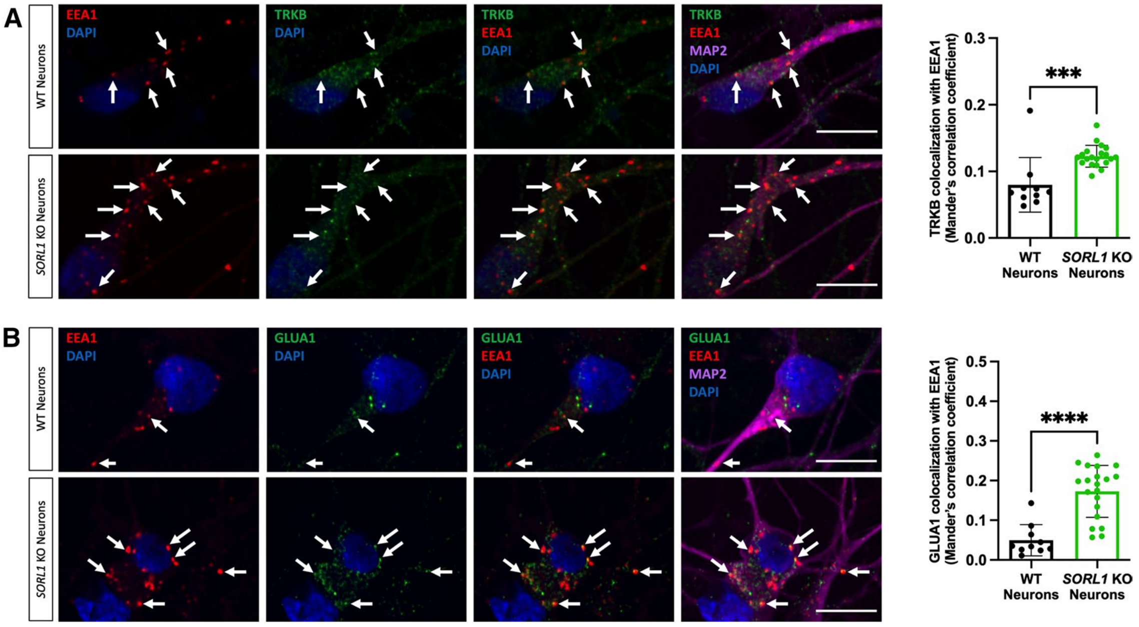

Fig. 1 Loss of *SORL1* expression leads to increased TRKB and GLUA1 localization in early endosomes. Representative immunofluorescent images of WT and *SORL1*KO neurons showing increased colocalization of **A** TRKB (green) and **B** GLUA1 (green) with EEA1 (red). All neurons were immunolabeled with MAP2 (far-red) and counterstained with DAPI (blue). Scale bar: 10 µm. In all cases, quantification of colocalization was represented as Mander's correlation co-efficient (MCC). 1 WT and 2 *SORL1*KO isogenic clones were used for these experiments and 10 images per clone per genotype were analyzed. Data represented as mean ± SD. Data were analyzed using parametric two-tailed unpaired *t* test. Significance was defined as a value of $^{*}p < 0.05$, $^{**}p < 0.01$, $^{***}p < 0.001$, and $^{****}p < 0.0001$

significant decrease in colocalization of TRKB (Fig. 2B) and GLUA1 (Fig. 2C) with Rab7. This result is consistent with our previous observation for APP [41]. We analyzed colocalization of these cargo with LAMP1 and we observed a significant decrease with APP (Fig. 2D) and TRKB (Fig. 2E) and a trend of a decrease with GLUA1 (Fig. 2F). These data indicate some fluidity in the network but suggest that trafficking of APP, TRKB and GLUA1 to late endosomes/lysosomes is all decreased by *SORL1*KO, although GLUA1 may be more likely to be trafficked to cell surface pathways or utilizes other adaptor proteins for late endosome to lysosomal trafficking. These changes in localization are not due to changes in expression of cargo. We have previously shown that APP levels do not change in *SORL1*KO neurons [42] and also show here that protein expression of TRKB and GLUA1 are not different (Supplemental Figure 3).

We next utilized previously generated cell lines that overexpress *SORL1* cDNA using the piggybac transposon system [96] to test whether increased *SORL1* expression may enhance the trafficking pathways that are impaired in the *SORL1*KO neurons. Importantly, the *SORL1* overexpressing (*SORL1*OE) cell line and control were generated in the same genetic background as our *SORL1*KO and isogenic WT cell lines. Interestingly, while there was no effect of *SORL1* overexpression on DQ Red BSA fluorescence at the earlier time point (6 h), we did see a significant enhancement of DQ RED BSA trafficking at the 24-h time point (Fig. 3A). In accordance, we observed significantly increased localization of our studied cargo with late endosomal and lysosomal markers in the *SORL1*OE neurons (Fig. 3B–G).

Lysosome size can influence lysosome function and is altered in AD [17, 38]. Similarly, location and number of lysosomes within neurons can alter degradative activity [11, 24, 28, 94] and in some cases, altered lysosomal distribution may represent an early neuropathological defect [98]. Recently, loss of *SORL1* in hiPSC neurons was shown to contribute to lysosome dysfunction as indicated by both increased lysosome size and number as well as decreased cathepsin-D activity [37]. Therefore, we first analyzed LAMP1-immunopositive puncta and also documented a significant increase in lysosome size and number in our *SORL1*KO neurons (Supplemental Figure 2A). Interestingly, although the number of lysosomes marked by LAMP1 puncta is increased in *SORL1KO* neurons, we did not observe a significant change in LAMP1 protein expression (Supplemental Figure 3). This may be partially explained by differences in autophagy in SORL1 KO neurons which we did not examine in this study but that has been previously reported [37] and further underscores the dynamic complexity of the endo-lysosomal network.

Next, we analyzed colocalization of Cathepsin-D and LAMP1 to determine if loss of *SORL1* expression leads to altered Cathepsin-D trafficking in neurons. Retromer trafficking is required to deliver one of the most abundant lysosomal proteases, pro-cathepsin D, to lysosomes via the mannose-6-phosphate receptor (M6PR) [64, 76]. The SORLA protein has a GGA-binding motif within its cytoplasmic domain similar to that of M6PR [39, 86], and mistrafficking of Cathepsin-D to lysosomes could affect the maturation and degradative capacity of these organelles. Therefore, we analyzed colocalization of Cathepsin-D and LAMP1 to determine if loss of *SORL1* expression leads to altered Cathepsin-D trafficking in neurons. However, we did not observe a change in Cathepsin-D colocalization between WT and *SORL*1KO (Supplemental Figure 2).

Taken together, our data suggest that *SORL1* loss in neurons reduces trafficking of cargo out of the early endosome to the late endosome and lysosome, contributing to lysosome stress as evidenced by an increase in size and number in these conditions while the decreased cathepsin-D activity observed upon *SORL1* loss [37] may not be due to impairment of lysosomal trafficking of the enzyme.

Loss of *SORL1* impacts the endosomal recycling pathway

Another route out of the early endosome is via the endocytic recycling complex (ERC) which can send cargo either to the cell surface or to the trans-Golgi network [29, 50, 52, 55]. To directly examine if *SORL1* expression alters recycling function, we performed a transferrin recycling assay using confocal microscopy. Transferrin can be recycled via a fast pathway within approximately 5–10 min after being internalized or via a slower pathway involving the ERC over longer periods of time [60, 85]. We examined the fluorescence intensity of Alexa Fluor 647-conjugated transferrin over a 40-min time course in WT and *SORL1*KO neurons and observed that a higher percentage of intracellular fluorescent transferrin persisted in *SORL1*KO neurons at both early and later time points as compared to WT neurons, indicating reduced recycling pathway function (Fig. 4A). Cargo destined for the cell surface can transit the ERC via Rab11 + recycling endosomes [69]. Altered size of recycling endosomes can be indicative of dysfunctional recycling of cargo through these compartments. We tested whether loss of *SORL1* expression affected the size of Rab11 + recycling endosomes. Interestingly, we observed a significant increase in the size of Rab11 + recycling endosomes, although there was no change in Rab11 protein expression in the *SORL1*KO neurons (Fig. 4B, Supplemental Figure 3), suggesting that this endosomal compartment is also under stress. To test if increased size is due to abnormal cargo trafficking through recycling endosomes, we assessed colocalization of APP, TRKB and GLUA1 with Rab11 and observed increased colocalization of all three cargoes with Rab11 + structures in *SORL1*KO neurons compared to WT neurons (Fig. 4C–E).

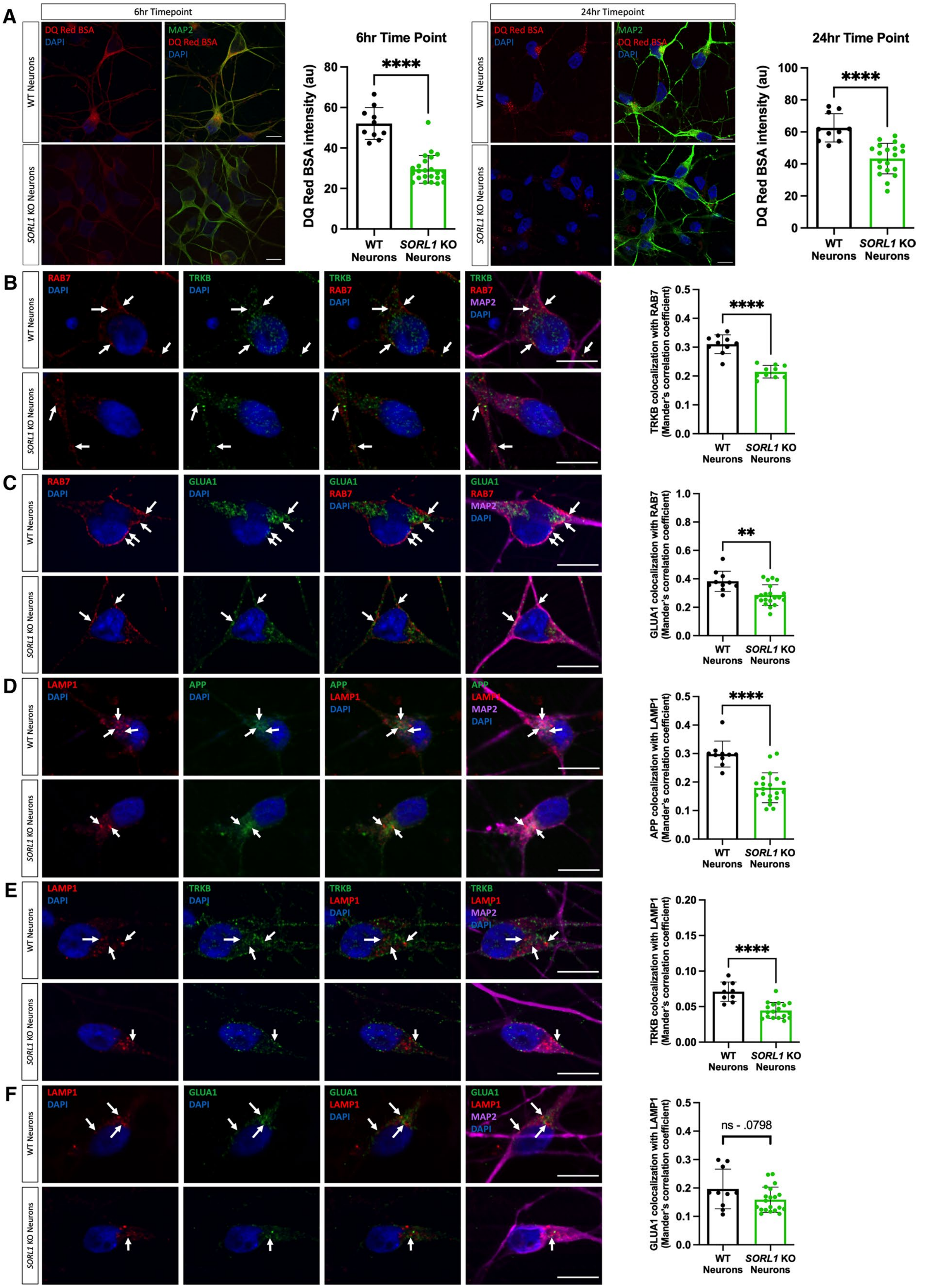
A
6hr Timepoint
WT Neurons
SORL1 KO Neurons
DQ Red BSA
DAPI
MAP2
DQ Red BSA
DAPI
6hr Time Point
DQ Red BSA intensity (au)
80
60
40
20
0
****
WT Neurons
SORL1 KO Neurons
24hr Timepoint
WT Neurons
SORL1 KO Neurons
DQ Red BSA
DAPI
MAP2
DQ Red BSA
DAPI
24hr Time Point
DQ Red BSA intensity (au)
100
80
60
40
20
0
****
WT Neurons
SORL1 KO Neurons
B
WT Neurons
SORL1 KO Neurons
RAB7
DAPI
TRKB
DAPI
TRKB
RAB7
DAPI
TRKB
RAB7
MAP2
DAPI
TRKB colocalization with RAB7 (Mander's correlation coefficient)
0.5
0.4
0.3
0.2
0.1
0.0
****
WT Neurons
SORL1 KO Neurons
C
WT Neurons
SORL1 KO Neurons
RAB7
DAPI
GLUA1
DAPI
GLUA1
RAB7
DAPI
GLUA1
RAB7
MAP2
DAPI
GLUA1 colocalization with RAB7 (Mander's correlation coefficient)
1.0
0.8
0.6
0.4
0.2
0.0
**
WT Neurons
SORL1 KO Neurons
D
WT Neurons
SORL1 KO Neurons
LAMP1
DAPI
APP
DAPI
APP
LAMP1
DAPI
APP
LAMP1
MAP2
DAPI
APP colocalization with LAMP1 (Mander's correlation coefficient)
0.5
0.4
0.3
0.2
0.1
0.0
****
WT Neurons
SORL1 KO Neurons
E
WT Neurons
SORL1 KO Neurons
LAMP1
DAPI
TRKB
DAPI
TRKB
LAMP1
DAPI
TRKB
LAMP1
MAP2
DAPI
TRKB colocalization with LAMP1 (Mander's correlation coefficient)
0.20
0.15
0.10
0.05
0.00
****
WT Neurons
SORL1 KO Neurons
F
WT Neurons
SORL1 KO Neurons
LAMP1
DAPI
GLUA1
DAPI
GLUA1
LAMP1
DAPI
GLUA1
LAMP1
MAP2
DAPI
GLUA1 colocalization with LAMP1 (Mander's correlation coefficient)
0.5
0.4
0.3
0.2
0.1
0.0
ns - .0798
WT Neurons
SORL1 KO Neurons

◂**Fig. 2** Loss of *SORL1* expression impairs trafficking to late endosomes and lysosomes. **A** *SORL1*KO neurons show reduced lysosomal proteolytic activity as measured by DQ Red BSA. Representative immunofluorescent images of WT and *SORL1*KO neurons showing double immunolabeling for MAP2 (green) and DQ Red BSA (red). Scale bar: 10 µm. Quantification of fluorescence intensity of DQ Red BSA using ImageJ software. **B**–**F** *SORL1*KO neurons show reduced colocalization of cargo with late endosomes and lysosomes. Representative immunofluorescent images of WT and *SORL1*KO neurons showing reduced colocalization of **B** TRKB (green) and **C** GLUA1 (green) with Rab7-positive late endosomes (red) in *SORL1*KO neurons. Representative immunofluorescent images of WT and *SORL1*KO neurons showing reduced colocalization of **D** APP (green) and **E** TRKB (green) and **F** GLUA1 (green) with LAMP1-positive lysosomes (red) in *SORL1*KO neurons. Scale bar: 10 µm. In all cases, quantification of colocalization was represented as Mander's correlation co-efficient (MCC). 1 WT and 2 *SORL1*KO isogenic clones were used for these experiments and 10 images per clone per genotype were analyzed. Data represented as mean ± SD. Data were analyzed using parametric two-tailed unpaired *t* test. Significance was defined as a value of $^{*}p < 0.05$, $^{**}p < 0.01$, $^{***}p < 0.001$, and $^{****}p < 0.0001$

Together, these data demonstrate that loss of *SORL1* impacts neuronal recycling endosome pathways by causing traffic jams in the recycling endosomes, similar to the effect that *SORL1* loss has on early endosomes.

SORL1 depletion reduces cell surface levels of cargo

Together, our data indicate that *SORL1*KO neurons have impaired cargo recycling with increased retention of cargo in recycling endosomes. These observations led us to test whether this cargo was indeed trafficked to the cell surface. A portion of APP has been shown to return to the cell surface via recycling endosomes [15] and SORLA can interact with the sorting nexin SNX27 to return APP to the cell surface [15, 35], although in that study the exact compartment was not described. Furthermore, recycling endosomes are the source for repopulation of AMPA receptors to the synapse during long-term potentiation [61]. We, therefore, examined cell surface levels of APP and GLUA1 using immunofluorescence and confocal microscopy. We documented a significant decrease in cell surface staining of both APP (Fig. 5A) and GLUA1 (Fig. 5B) in *SORL1*KO neurons as compared to WT, consistent with our hypothesis that SORLA is involved in regulating traffic from recycling endosomes. Due to the importance of GLUA1 in the formation of functional excitatory synapses, we next analyzed neuronal activity by culturing *SORL1*KO and isogenic WT neurons on multi-electrode array (MEA) plates. Interestingly, we observed an early increase in the mean firing rate of *SORL1*KO neurons at an early time point (27 days post-plating); however, neuronal firing in *SORL1*KO neurons was significantly reduced at a later time point (66 days post-plating) (Fig. 5C) suggesting that synaptic activity may be partially impaired in these cells.

SORL1 overexpression enhances endosomal recycling

Defects in cell surface recycling have severe consequences in neurons, especially as these processes are necessary for healthy neuronal function and enhancing pathways that promote endosomal recycling in neurons may be beneficial. Using our *SORL1*OE neurons, we analyzed recycling function using the transferrin recycling assay and observed that *SORL1*OE neurons showed significantly faster transferrin recycling (Fig. 6A). We next tested whether colocalization of cargo with recycling endosomes and cell surface recycling was altered between *SORL1*OE and WT neurons. Interestingly, the size of Rab11 + recycling endosomes was significantly smaller in *SORL1*OE neurons (Fig. 6B) possibly indicating that increased *SORL1* expression is clearing cargo more rapidly from this compartment. We observed a significant increase in localization of cargo with Rab11 + recycling endosomes (Fig. 6C–E). While this result was initially surprising, as we also saw increased colocalization with Rab11 + recycling endosomes in our *SORL1*KO neurons (Fig. 4C–E), we further documented a significant increase of APP and GLUA1 on the cell surface compared to WT neurons with only endogenous *SORL1* expression (Fig. 6F, G), as opposed to decreased APP and GLUA1 localization on the cell surface in *SORL1*KO neurons (Fig. 5A, B). These results suggest that cell surface trafficking via a Rab11 pathway is enhanced by increased *SORL1* expression and that a crucial action of SORLA is the trafficking out of recycling endosomes. Thus, our data support a critical role for SORLA for trafficking cargo from recycling endosomes to the cell surface. In addition, we show for the first time that SORLA levels may regulate cell surface recycling of AMPA receptor subunits in human neurons.

SORL1 depletion affects gene expression

To determine a more global effect of chronic *SORL1* loss in human neurons, we performed bulk RNA sequencing of *SORL1*KO neurons compared to WT neurons. Interestingly, we observed that there were significantly more downregulated genes in *SORL1*KO neurons than upregulated ones (Supplemental Figure 4B). While none of the cargo we explicitly studied in this work was differentially expressed, GO analysis showed that the top downregulated molecular function pathways in the *SORL1*KO cells were related to receptor–ligand activity and extracellular matrix organization (Fig. 7A). The top upregulated molecular function pathways were related to ion channel activity (Fig. 7B). To understand these data in the context of an integrated network, we used an analysis method that infers ligand receptor

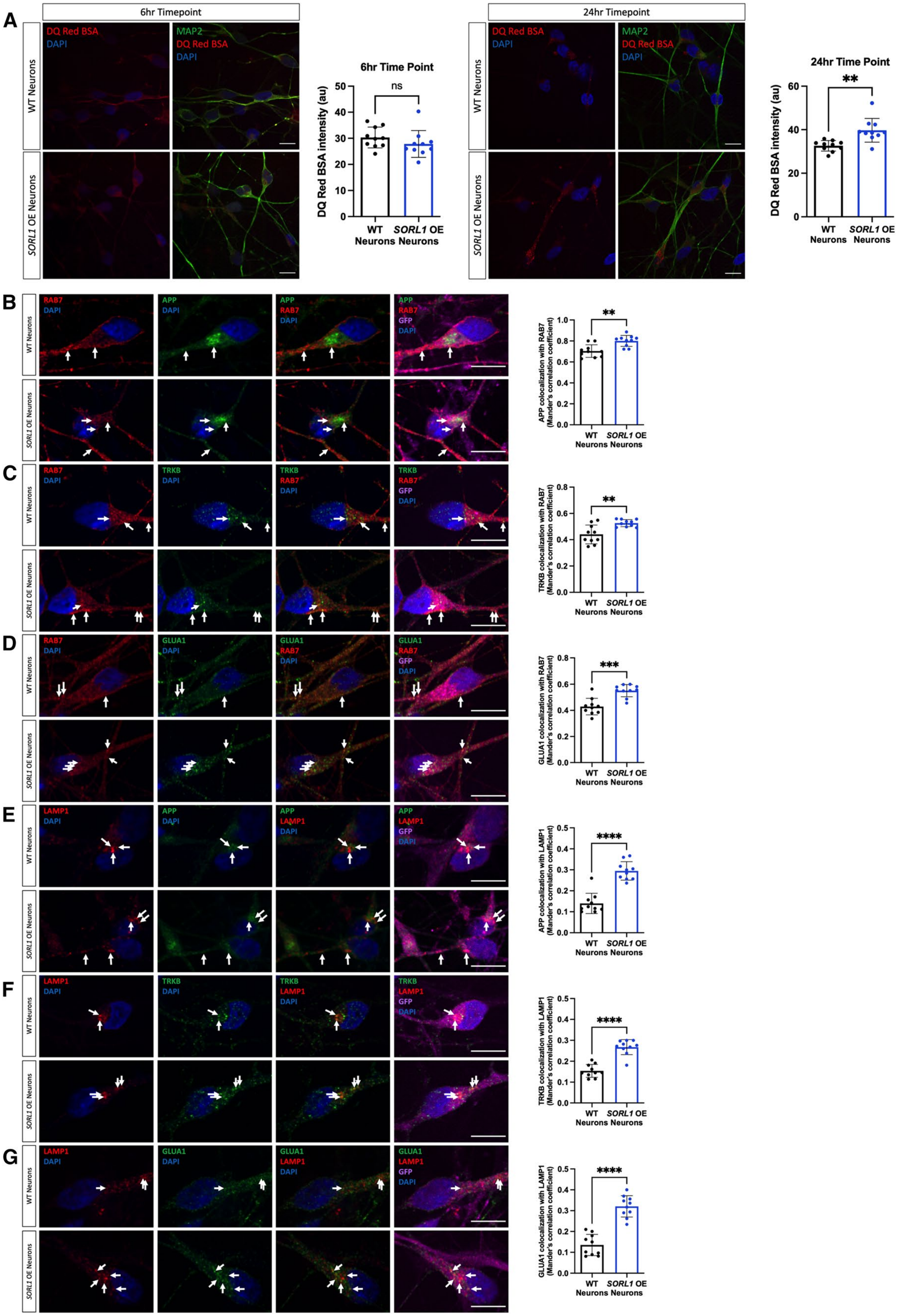
A
6hr Timepoint
DQ Red BSA
DAPI
MAP2
DQ Red BSA
DAPI
WT Neurons
SORL1 OE Neurons
6hr Time Point
ns
DQ Red BSA intensity (au)
0
10
20
30
40
50
WT Neurons
SORL1 OE Neurons
24hr Timepoint
24hr Time Point
**
0
20
40
60
B
RAB7
DAPI
APP
GFP
APP colocalization with RAB7 (Mander's correlation coefficient)
**
C
TRKB
TRKB colocalization with RAB7 (Mander's correlation coefficient)
**
D
GLUA1
GLUA1 colocalization with RAB7 (Mander's correlation coefficient)
***
E
LAMP1
APP colocalization with LAMP1 (Mander's correlation coefficient)
****
F
TRKB colocalization with LAMP1 (Mander's correlation coefficient)
****
G
GLUA1 colocalization with LAMP1 (Mander's correlation coefficient)
****

◂**Fig. 3** Enhancing *SORL1* expression improves trafficking to late endosomes and lysosomes. **A** *SORL1*OE neurons show no change in lysosomal proteolytic activity as measured using DQ Red BSA after a 6 h treatment but do show an enhancement of trafficking at 24 h. Representative immunofluorescent images of WT and *SORL1*OE neurons showing double immunolabeling for MAP2 (green) and DQ Red BSA (red). Scale bar: 10 µm. Quantification of fluorescence intensity of DQ Red BSA using ImageJ software. 1 cell line of each genotype (WT vs. SORL1 OE) was used for these experiments. 10 images per genotype were analyzed. Representative immunofluorescent images of WT and *SORL1*OE neurons showing increased colocalization of APP, TRKB and GLUA1 (green) with Rab7 (red) (**B**–**D**) and LAMP1 (red) (**E**–**G**) in *SORL1*OE neurons. *SORL1*OE neurons and controls have endogenous GFP expression due to the piggybac vector system. GFP fluorescence is pseudo-colored (Far-red) and was used to outline cell bodies. Scale bar: 10 µm. Nuclei are counterstained with DAPI (blue). In all cases, quantification of colocalization was represented as Mander's correlation co-efficient (MCC). 1 cell line of each genotype (WT vs. SORL1 OE) was used for these experiments. 10 images per genotype were analyzed. Data represented as mean ± SD. Data were analyzed using parametric two-tailed unpaired *t* test. Significance was defined as a value of $^{*}p < 0.05$, $^{**}p < 0.01$, $^{***}p < 0.001$, and $^{****}p < 0.0001$

interactions from bulk RNA-seq data [67, 92]. We observed several nodes of altered receptor–ligand interactions that indicate altered cell surface recycling and neurotrophic activity (Fig. 7C). These include alterations in β-integrin signaling, which is consistent with previous work showing reduced β-integrin on the cell surface in *SORL1*KO cancer cells [63], and altered interactions in ephrins/ephrin receptors, also corroborating previous work implicating *SORL1* expression in ephrin signaling and synapse regulation [34]. Our analysis also showed nodes with alterations in nerve growth factor/nerve growth factor receptor (NGF/NGFR) and fibroblast growth factor/fibroblast growth factor receptor (FGF/FGFR) signaling, indicating alterations in neurotrophin and growth factor signaling and suggesting that the presence of endosomal traffic jams in *SORL1*KO neurons may ultimately impact multiple pathways important for neuronal health and development. Since we documented a decrease of GLUA1 puncta on the cell surface and observed altered neuronal activity on MEAs, we further mined our RNA-seq data for genes involved in synaptic function. Interestingly when we performed enrichment analysis, we observed that pathways associated with synaptic function were upregulated in *SORL1*KO neurons (Supplemental Figure 5).

Discussion

Trafficking through the endo-lysosomal network regulates intracellular location of proteins, dictating their homeostasis, function and influence on cellular physiology. Functional studies by our group and others document endosomal abnormalities in hiPSC-derived neuronal models of AD [37, 42, 44]. Emerging from this evidence is the role of *SORL1* as an endosomal gene that plays essential roles in mediating cargo trafficking. Recent work has implicated *SORL1* as AD's fourth causal gene [5, 73], and of these genes, it is the only one linked to the common late-onset form of the disease. Understanding *SORL1*'s function is paramount for understanding AD's pathogenic mechanisms and for potential therapeutic interventions.

Acting as an adaptor molecule of the retromer trafficking complex, SORLA has already been pathogenically linked to AD by its role in recycling APP out of endosomes [4, 31, 59]. This current work and our previous study [42] shows that *SORL1* depletion leads to increased APP localization in early and recycling endosomes. By lengthening the residence time of APP in these endosomal compartments, accelerated amyloidogenic cleavage of APP occurs due to the close proximity of APP and BACE1 [87]. Indeed, loss of *SORL1* leads to the accumulation of Aβ peptides, an antecedent of 'amyloid pathology' [4, 42, 70]. We hypothesized that loss of *SORL1* in neurons would impact other cargo important for healthy neuronal function. To test this hypothesis, in addition to APP, we examined localization of the neurotrophin receptor TRKB and the GLUA1 subunit of the AMPA receptor and also observed that these proteins are increased in early endosomes (Fig. 1). These cargoes link to another key pathology of AD: neurodegeneration, a slowly progressive process that begins with synaptic dysfunction characterized by glutamate receptor loss, which then progresses to synaptic loss before ultimately, over years, leading to widespread neuronal cell death [78].

The early endosome is considered the central station in the sorting and trafficking of cargo throughout the many stations of the endo-lysosomal system. While the early endosome is the station that is affected first and foremost in AD, it is not surprising that a primary dysfunction in this central station will secondarily influence trafficking throughout the system including the recycling and degradative pathways. Indeed, SORLA was shown to traffic Aβ to lysosomes in neuroblastoma cells, a function that is impaired by an AD-associated variant [8]. Our work presented in this study, along with other recent work [37] also supports a role for *SORL1* in lysosomal trafficking in neurons. We observe a decrease in the pH-sensitive fluorogenic substrate DQ RED BSA in our *SORL1*KO neurons and decreased localization of APP, TRKB, and GLUA1 in late endosomes and lysosomes in *SORL1*KO neurons and that this is reversed in *SORL1*OE neurons (Figs. 2, 3). We interpret our functional and colocalization data to suggest that loss of *SORL1* expression mainly affects trafficking of cargo to lysosomes, but our data do not rule out a role of SORLA in neuronal lysosome function. Hung et al. reported decreased Cathepsin-D activity in *SORL1*-deficient neurons, suggesting that *SORL1* loss directly impacts lysosome function [37]. While we did

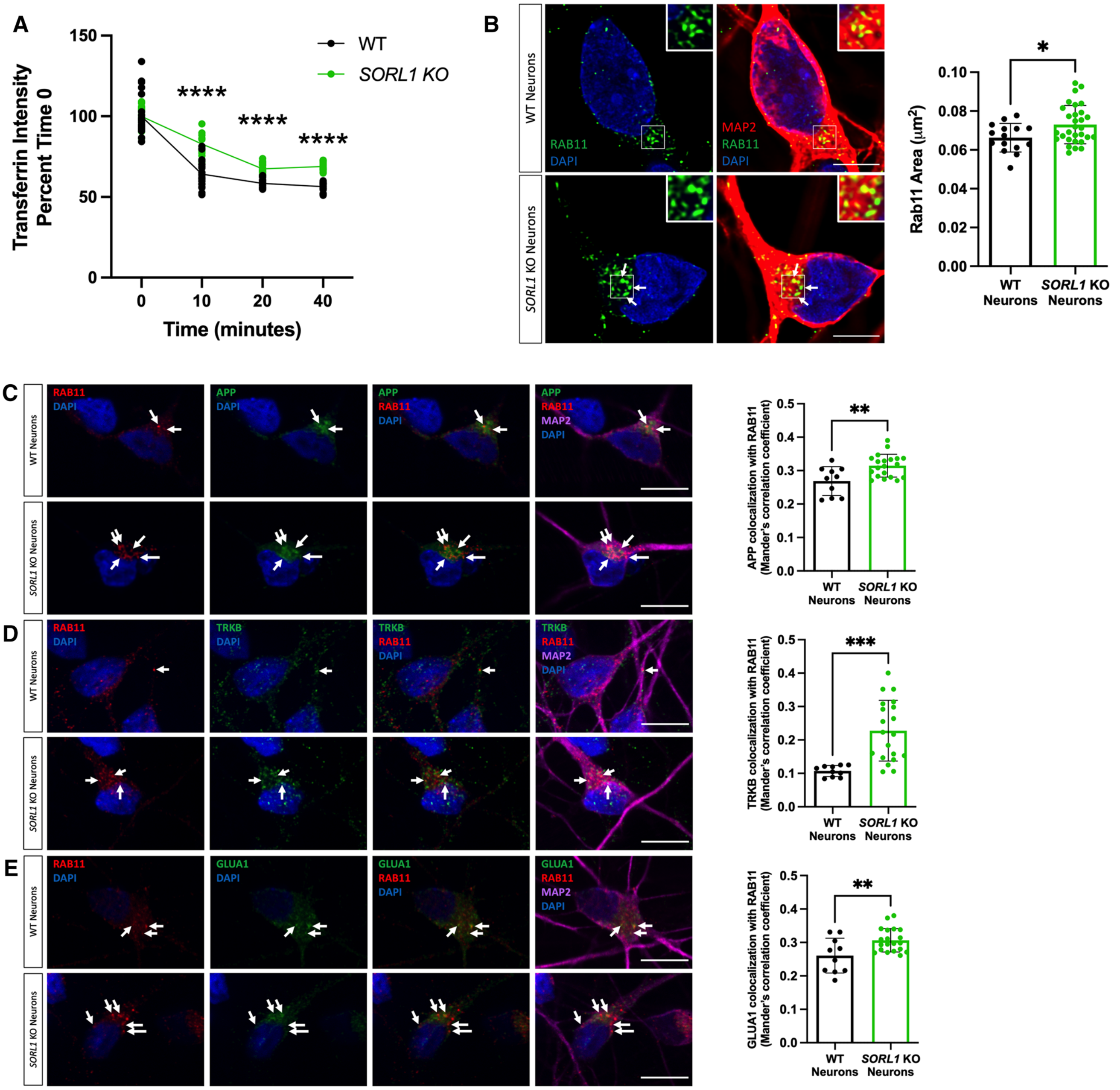

Fig. 4 Loss of *SORL1* impacts the cell surface recycling pathway. **A** *SORL1*KO neurons show slower rate of transferrin recycling. Quantification of fluorescence intensity of intracellular transferrin at different time points after treating cells with Alexa Fluor 647-conjugated transferrin for 15 min, using ImageJ software. Data represented as percent of time 0 fluorescence intensity. 2 WT and 2 *SORL1*KO isogenic clones were used for these experiments. 12 images per clone per genotype were analyzed. **B** *SORL1*KO neurons show larger recycling endosomes. Representative immunofluorescent images of WT and *SORL1*KO neurons labeled with antibodies for MAP2 (red) and Rab11 (green). Nuclei were counterstained with DAPI (blue). Scale bar: 5 μm. Quantification of size of Rab11-labeled recycling endosomes using CellProfiler software. 1 WT and 2 *SORL1*KO isogenic clones were used for these experiments. 15 images per clone per genotype were analyzed. Representative immunofluorescent images of WT and *SORL1*KO neurons showing increased colocalization of **C** APP (green), **D** TRKB (green) and **E** GLUA1 (green) with Rab11-positive recycling endosomes (red) in *SORL1*KO neurons. Scale bar: 10 μm. In all cases, quantification of colocalization was represented as Mander's correlation co-efficient (MCC). 1 WT and 2 *SORL1*KO isogenic clones were used for these experiments. 10 images per clone per genotype were analyzed. Data represented as mean ± SD. Data were analyzed using parametric two-tailed unpaired *t* test and two-was ANOVA. Significance was defined as a value of $^{*}p < 0.05$, $^{**}p < 0.01$, $^{***}p < 0.001$, and $^{****}p < 0.0001$

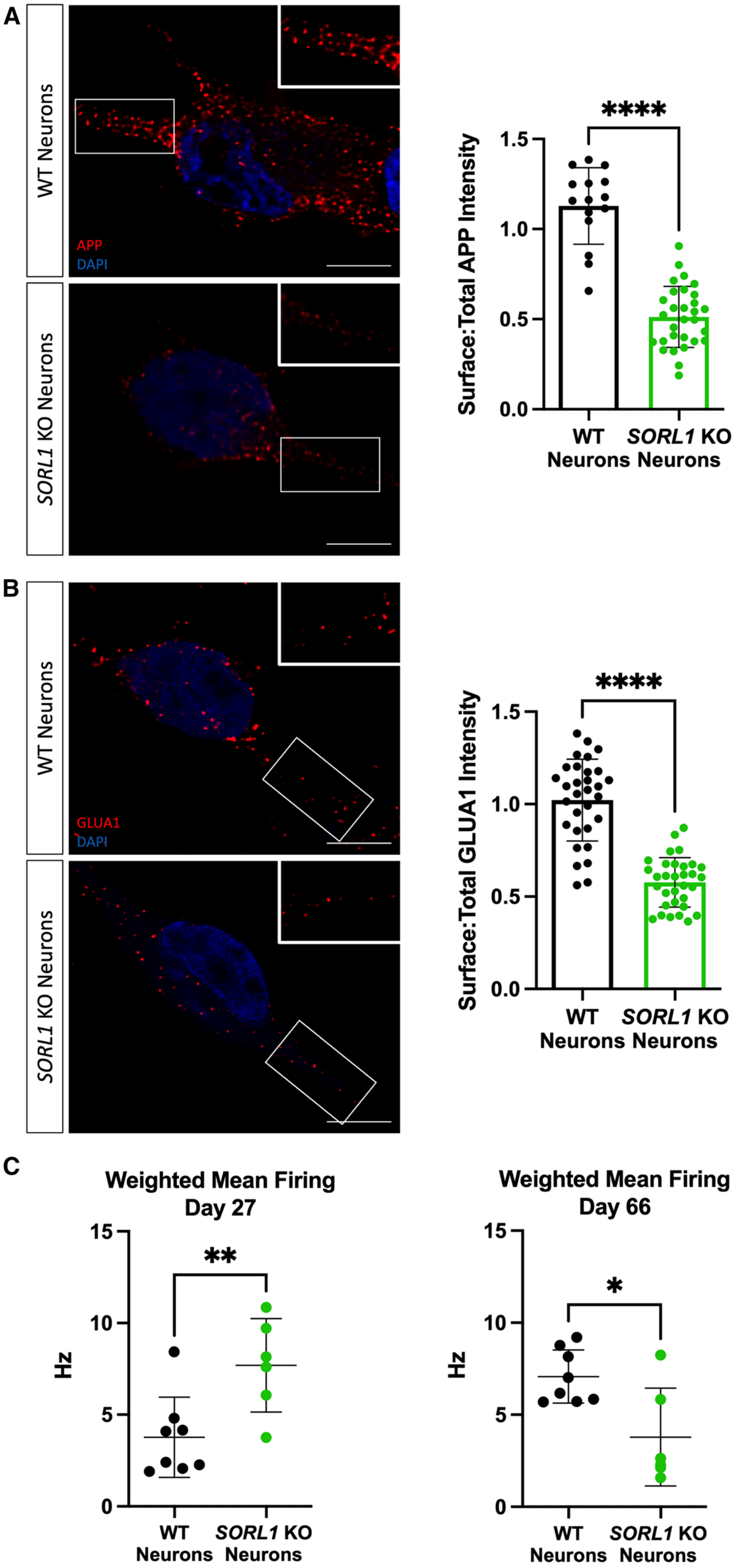

Fig. 5 Loss of *SORL1* expression impairs recycling to the cell surface. **A**–**B** *SORL1*KO neurons show reduced cell surface expression of APP (**A**) and GLUA1 (**B**). Representative immunofluorescent images of WT and *SORL1*KO neurons labeled with antibodies for APP (**A**) (red) and GLUA1 (**B**) (red). Scale bar: 5 µm. Intensity of APP and GLUA1 measured using ImageJ software. Data are presented as a ratio of surface intensity to total intensity. 2 WT and 2 *SORL1*KO clones were used in these experiments. 16 images per clone per genotype were analyzed. Data represented as mean ± SD. Normally distributed data were analyzed using parametric two-tailed unpaired *t* test. Significance was defined as a value of $^{*}p<0.05$, $^{**}p<0.01$, $^{***}p<0.001$, and $^{****}p<0.0001$. **C** Multielectrode array (MEA) analysis of WT and *SORL1*KO neurons at early (d27) and late (d66) time points of differentiation. 1 WT and 1 *SORL1*KO clone was used for these experiments. Data represented as mean ± SD. Data were analyzed using parametric two-tailed unpaired *t* test. Significance was defined as a value of $^{*}p<0.05$, $^{**}p<0.01$, $^{***}p<0.001$, and $^{****}p<0.0001$

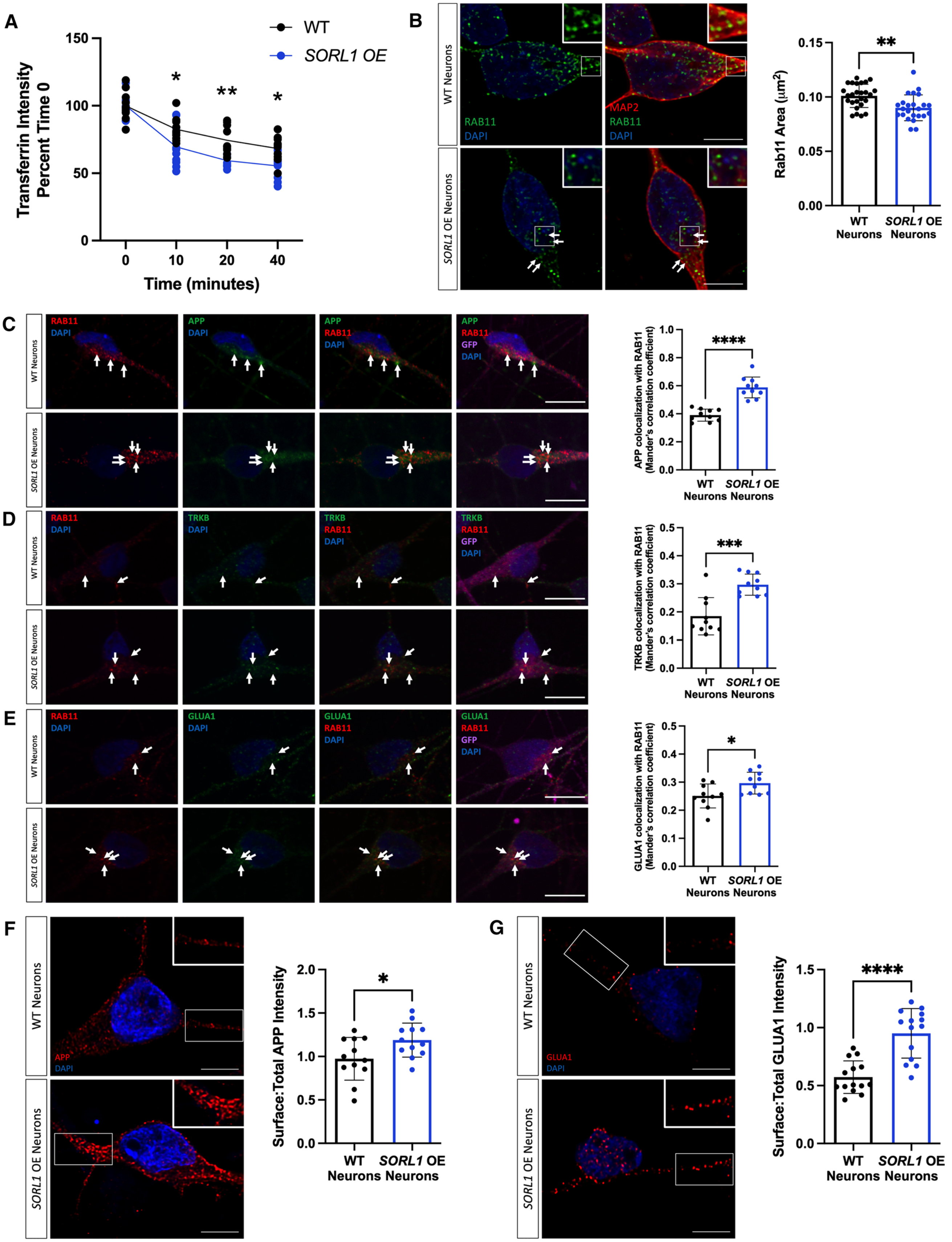
A
WT
SORL1 OE
Transferrin Intensity Percent Time 0
150
100
50
0
0
10
20
40
Time (minutes)
*
**
*
B
WT Neurons
SORL1 OE Neurons
RAB11
DAPI
MAP2
RAB11
DAPI
Rab11 Area (μm²)
0.15
0.10
0.05
0.00
**
WT Neurons
SORL1 OE Neurons
C
WT Neurons
SORL1 OE Neurons
RAB11
DAPI
APP
DAPI
APP
RAB11
DAPI
APP
RAB11
GFP
DAPI
APP colocalization with RAB11 (Mander's correlation coefficient)
1.0
0.8
0.6
0.4
0.2
0.0
****
WT Neurons
SORL1 OE Neurons
D
WT Neurons
SORL1 OE Neurons
RAB11
DAPI
TRKB
DAPI
TRKB
RAB11
DAPI
TRKB
RAB11
GFP
DAPI
TRKB colocalization with RAB11 (Mander's correlation coefficient)
0.5
0.4
0.3
0.2
0.1
0.0
***
WT Neurons
SORL1 OE Neurons
E
WT Neurons
SORL1 OE Neurons
RAB11
DAPI
GLUA1
DAPI
GLUA1
RAB11
DAPI
GLUA1
RAB11
GFP
DAPI
GLUA1 colocalization with RAB11 (Mander's correlation coefficient)
0.5
0.4
0.3
0.2
0.1
0.0
*
WT Neurons
SORL1 OE Neurons
F
WT Neurons
SORL1 OE Neurons
APP
DAPI
Surface:Total APP Intensity
2.0
1.5
1.0
0.5
0.0
*
WT Neurons
SORL1 OE Neurons
G
WT Neurons
SORL1 OE Neurons
GLUA1
DAPI
Surface:Total GLUA1 Intensity
1.5
1.0
0.5
0.0
****
WT Neurons
SORL1 OE Neurons

◂**Fig. 6** Overexpression of *SORL1* enhances endosomal recycling. **A** *SORL1*OE neurons show faster rate of transferrin recycling. Quantification of fluorescence intensity of intracellular transferrin at different time points after treating cells with Alexa Fluor 647-conjugated transferrin for 15 min, using ImageJ software. Data represented as percent of time 0 fluorescence intensity. 1 cell line of each genotype (WT vs. SORL1 OE) was used for these experiments. 10 images per genotype were analyzed. **B** *SORL1*OE neurons show reduced size of recycling endosomes. Representative immunofluorescent images of WT and *SORL1*OE neurons labeled with Rab11 (green) and MAP2 (red) showing smaller Rab11-positive recycling endosomes in *SORL1*OE neurons. Nuclei counterstained with DAPI (blue). Quantification of Rab11 + recycling endosome size performed using Cell Profiler software and represented as area of Rab11 + vesicles. Scale bar: 5 µm. 1 cell line of each genotype (WT vs. SORL1 OE) was used for these experiments. 26 images per genotype were analyzed. Representative immunofluorescent images of WT and *SORL1*OE neurons showing increased colocalization of **C** APP (green), **D** TRKB (green) and **E** GLUA1 (green) with Rab11 (red)-positive recycling endosomes. *SORL1*OE neurons and controls have endogenous GFP expression due to the piggybac vector system. GFP fluorescence is pseudo-colored (Far-red) and was used to outline cell bodies. Quantification of colocalization with Rab11 represented as Mander's Correlation Co-efficient (MCC). Scale bar: 10 µm. 1 cell line of each genotype (WT vs. SORL1 OE) was used for these experiments. 10 images per genotype were analyzed. Representative immunofluorescent images of WT and *SORL1*OE neurons showing increased cell surface expression of **F** APP (red) and **G** GLUA1 (red) in *SORL1*OE neurons. Scale bar: 5 µm. Fluorescence intensity of APP and GLUA1 measured using ImageJ software. Data are presented as a ratio of surface intensity to total intensity. Nuclei counterstained with DAPI. 1 cell line of each genotype (WT vs. SORL1 OE) was used for these experiments. 12–14 images per genotype were analyzed. Data represented as mean ± SD. Data were analyzed using parametric two-tailed unpaired *t* test and two-way ANOVA. Significance defined as a value of $*p < 0.05$, $**p < 0.01$, $***p < 0.001$, and $****p < 0.0001$

not observe a difference in Cathepsin-D localization to lysosomes, it is important to note that LAMP1 only partially colocalizes with Cathepsin-D in neurons [11]. Furthermore, the loss of proteolytic activity evidenced by decreased intensity of DQ Red BSA in *SORL1*KO neurons may not be completely due to reduced trafficking to lysosomes but could be a result of abnormal lysosomal function as DQ Red BSA is internalized by a process called macropinocytosis wherein macropinosomes can be directly trafficked to lysosomes [30, 49, 65]. Interestingly, while we did not observe an effect on DQ Red BSA at a shorter time point in *SORL1*OE neurons, we did see increased fluorescence of this reagent at a 24-h time point (Fig. 3), suggesting that over time, increased SORL1 expression impacts lysosome trafficking and/or function in cortical neurons.

Our experiments also point to *SORL1*'s role in cell surface recycling. Using a prototypical cargo, transferrin, we demonstrate a reciprocal role between loss and enhancement of *SORL1* expression in cell surface recycling. Specifically, we show that *SORL1*KO neurons have defects in transferrin recycling at both early (10 min) and late (40 min) time points while *SORL1*OE neurons have faster recycling at these time points (Figs. 4, 6). This suggests that SORLA functions in both fast and slow endosomal recycling. Our data further implicates the recycling pathway by showing that modulation of SORLA expression affects recycling endosome size and the amount of cargo (APP, TRKB and GLUA1) localized to recycling endosomes (Figs. 4, 6).

Endocytic recycling comprises returning cargo, primarily membrane proteins, to the cell surface [14]. We studied a canonical SORLA cargo, APP, and show that loss of *SORL1* expression results in reduced cell surface APP while enhanced expression increases cell surface APP (Fig. 5). These results corroborate previous work showing that *SORL1* and SNX27 work to return APP to the cell surface [15, 35] in a human model.

We also show that *SORL1* plays a role in recycling glutamate receptors in human neurons (Fig. 5). This finding is critically important as recent work indicates that in mouse cortical neurons, SORLA interacts with a neuronal specific retromer subunit, VPS26b, to promote recycling of glutamate receptors [80]. In our cortical neurons when *SORL1* is depleted, there is a reduction of GLUA1 subunits on the cell surface and this may result in synaptic impairment. MEA data comparing *SORL1*KO and isogenic WT neurons shows alterations in weighted mean firing rate as neurons mature (Fig. 5). Interestingly, we observed an increase in neuronal firing at an early time point and a significant decrease in firing at a later time point. *SORL1*KO mice live to adulthood but have been described to have some deficits in learning and memory that may also be age dependent [27, 32]. Some of these alterations could be explained by compensatory expression changes of ion channels or synaptic genes induced by chronic loss of *SORL1* during the course of neuronal differentiation from pluripotent stem cells. Our RNA-seq data do show upregulation of ion channels and channel activity (Fig. 7). Interestingly, when we further interrogated our RNA-seq data for pathways enriched in synaptic function using the SynGo database [43], we observed an upregulation of differentially expressed genes in synaptic pathways (Supplemental Figure 5). This data suggests that *SORL1*KO neurons may attempt to compensate for altered trafficking of synaptic receptors by upregulating gene expression.

Our unbiased transcriptomic screen further supported that neurotrophic signaling and cell surface recycling pathways are impacted by *SORL1* deficiency (Fig. 7). In one study, the SORLA cytoplasmic tail was observed to translocate to the nucleus and activate transcription in a reporter gene assay [6]. Another possibility is that due to its effects on APP cleavage, *SORL1* levels may influence the APP intracellular domain (AICD) which is known to affect gene transcription [58]. Despite this, distinct genes regulated by SORLA are not known. Rather than looking for a direct effect on gene regulation, our goal for the analysis was to determine the global effect of *SORL1* loss or overexpression on neuronal

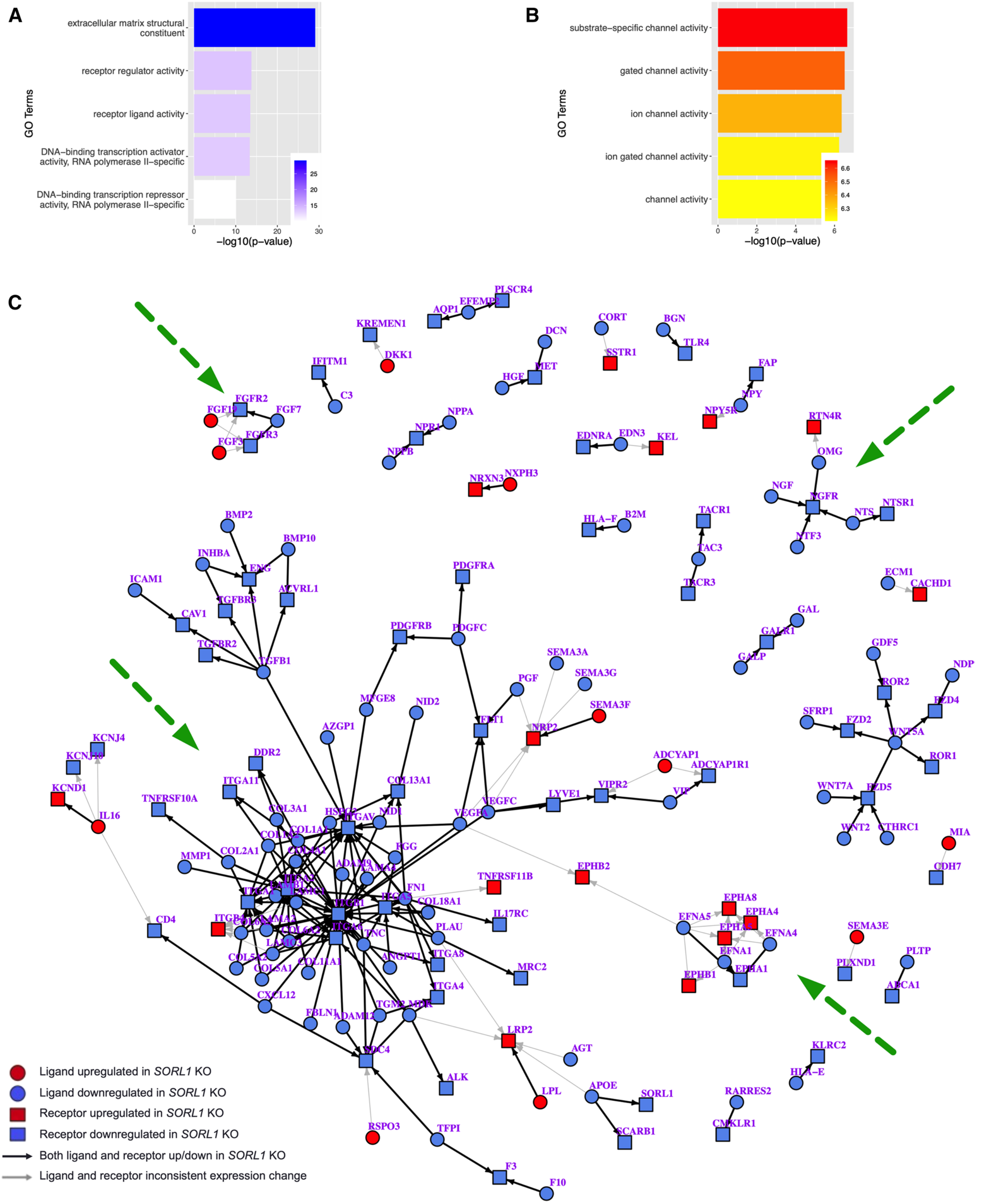

networks. Indeed, our data does not show that the specific cargo proteins described here are differentially expressed. However, the analysis does indicate that loss of *SORL1* in human neurons impacts cell surface networks, including receptor ligand interactions in neurotrophic and growth factor pathways, β-integrin signaling, and ephrin signaling.

◂**Fig. 7** Analysis of bulk RNA-sequencing data indicates alterations in cell surface and extracellular trafficking, receptor–ligand and channel activity. Gene ontology analysis of DEGs in WT and *SORL1*KO neurons. Shown here are the top upregulated (**A**) and downregulated (**B**) molecular function terms in *SORL1*KO neurons. GO annotation terms are listed on the y-axis, adjusted p-value is shown on the *x*-axis. (**C**) Ligand–receptor network changes in *SORL1*KO neurons, identified if genes are more than 1.5-fold increased or decreased in *SORL1*KO neurons with an adjusted p-value less than 0.05. Circles denote ligands, squares denote receptors, blue indicates genes expressed significantly lower in *SORL1*KO neurons, red indicates genes expressed significantly higher in *SORL1*KO neurons. Arrows point from ligand to receptor, denoting receptor–ligand interactions. Black arrows denote consistent expression changes between ligand and receptor, indicating that both genes in the pair are either upregulated or downregulated. Gray arrows denote inconsistent changes between ligand and receptor. Clusters impacted by cell surface recycling (β-integrins, ephrins) or neurotrophic signaling (FGF/FGFR, NGF/NGFR) are indicated by green dotted arrows. RNA was collected from 3 separate differentiations including a combination of two WT clones and two *SORL1*KO clones. Each sample includes 2–3 technical replicates

This corroborates previous work and the altered networks we observe impact neuronal health, axonal guidance, and synapse formation [34, 36, 63].

Importantly, enhancing SORL1 expression improves cell surface trafficking of GLUA1 (Fig. 6). Trafficking of glutamate receptors is an event that is critical for preventing synaptic dysfunction and synaptic loss, thus our results link *SORL1* to AD's early-stage neurodegenerative process. Since retromer-dependent glutamate receptor recycling has been shown to occur independent of APP [88], our previous and current results suggest that reduced *SORL1* activity can, at least in principle, drive two key AD pathologies, amyloid pathology and synaptic pathology, through parallel mechanisms [84].

We summarize our findings in relation to our previous work [42] in Fig. 8. In general, our results in human neurons corroborate studies in other cellular and animal models that implicate SORL1 as a key player in endosomal trafficking and recycling [1, 22, 31, 63, 82]. However, our study

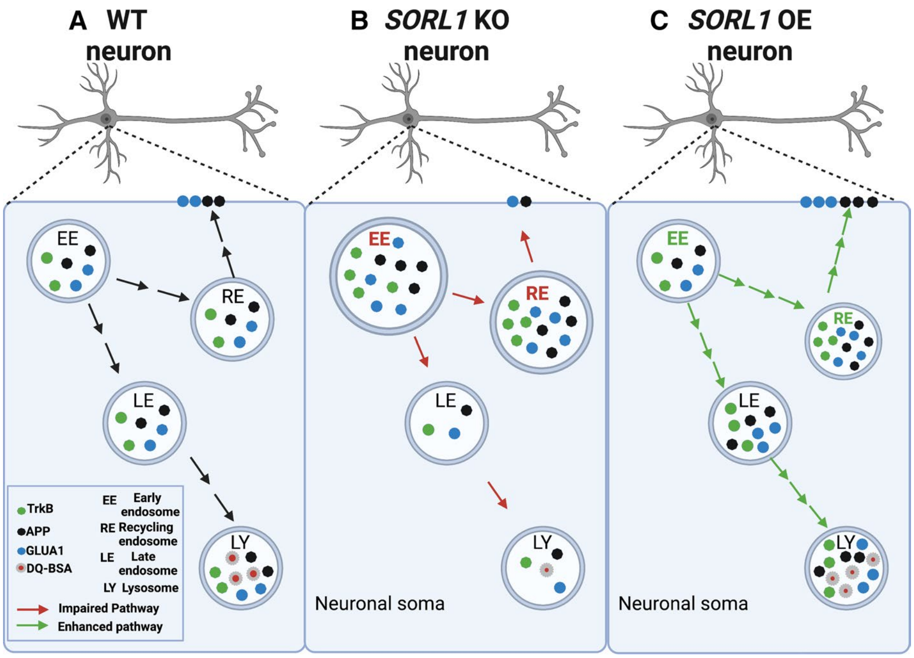

Fig. 8 Model of modulation of SORL1 expression in hiPSC-derived cortical neurons. Modulation of SORLA expression regulates endosomal recycling and degradative pathways in hiPSC-derived neurons: the early endosome is a sorting hub where various cargo can be trafficked to degradative or cell surface recycling pathways in neurons (**A**). In this study, we mapped trafficking of three important neuronal cargo under conditions of depletion (**B**) or enhancement (**C**) of the AD risk gene SORL1/SORLA. As depicted in panel **B**, our data suggest that modulation of SORL1 expression significantly impacts the neuronal recycling pathway because loss of SORL1 causes endosomal traffic jams indicated by swelling and enlargement of early [42] and recycling endosomes (Indicated in red arrows, bolded font) with accumulation of cargo in in SORL1 KO neurons compared to isogenic WT cells. Loss of SORL1 impacts recycling to the cell surface because, while there is increased cargo in recycling endosomes, there is a reduction of this cargo on the neuronal surface. Loss of SORL1 also impacts the degradative pathway out of the early endosome as there is a reduction of cargo in late endosome and lysosomes. As depicted in panel C, enhancement of SORL1 expression reciprocally impacts these pathways (Indicated in green arrows, bolded font). SORL1 OE neurons also have an increase in cargo in recycling endosomes, but unlike KO cells, this results in more cell surface trafficking of neuronal cargo, leading to reduced stress (small size) of recycling endosomes. In addition, SORL1 OE enhances trafficking out of the early endosome towards the degradative pathway as well. Taken together, our data solidify the AD risk gene SORL1 as a key modulator of neuronal endosomal trafficking. Created with Biorender.com

has certain limitations. Endosomal trafficking, in particular endosomal recycling, is a complex process. Because of its known genetic risk for AD, we specifically focused on the impact of modulating *SORL1* expression in human neurons on this pathway. However, many other factors, some of which may be independent of *SORL1*, may also impact this process. Dissecting these mechanisms in multiple model systems will be important for both basic and preclinical neurobiology. Furthermore, our results encompass only one human genome. Future studies will benefit from looking at *SORL1* deficiency or overexpression in multiple human genetic backgrounds. Furthermore, in this work we are describing purely neuronal phenotypes although *SORL1* is expressed in other CNS cells. Future work looking at cell autonomous and non-cell autonomous mechanisms of *SORL1* depletion or overexpression in human glial or brain organoid models will be informative.

Conclusions

In this work, we report that *SORL1* depletion impair endosomal trafficking leading to retaining of cargo in early and recycling endosomes and impacts cell surface recycling and lysosomal trafficking of neuronal cargo. In particular, we demonstrate that *SORL1* expression in neurons affects cell surface localization of GLUA1, with an impact on synaptic activity clearly highlighting the importance of SORL1 for the endosomal recycling pathways in neurons. This phenotype may ultimately translate to synaptic dysfunction and neurodegeneration as occurring in AD. Interestingly, increasing *SORL1* expression enhances endosomal recycling and increases cell surface GLUA1. While the secondary downstream effects induced by *SORL1* depletion in the endo-lysosomal system are interesting and likely relevant to AD's ultimate pathogenesis, from a therapeutic perspective it is best to target *SORL1*'s primary defect, which seems to localize to the endosomal recycling pathway. Interestingly, recent biomarker studies suggest that defects in retromer-dependent endosomal recycling occur in a majority of patients with 'sporadic' AD [81], suggesting that the observed *SORL1*-induced defects may generalize across early- and late-onset forms of the disorder. Collectively, our results support the conclusion that *SORL1*, and the retromer-dependent pathway in which it functions, is a valid therapeutic target and interventions directed at this pathway may ameliorate endosomal recycling defects that seem to act as, at least, one primary driver of AD.

Supplementary Information The online version contains supplementary material available at https://doi.org/10.1007/s00018-022-04182-9.

Acknowledgements We thank Dr. Harald Frankowski, Dr. Yoshito Kinoshita, Ms. Shannon Rose, Ms. Eden Cruickshank and all members of the Young Laboratory for critical discussions and feedback during the preparation of this manuscript. We also thank Dr. Scott A. Small and Dr. Gregory A. Petsko for critical comments, discussions and feedback on this work. We would like to acknowledge the UW SLU Cell Analysis Facility and the Garvey Imaging Core at the UW Institute for Stem Cell and Regenerative Medicine. This work was supported by a NIH grant (R01AG062148) and a BrightFocus Foundation grant (A2018656S) to J.E.Y., a Biogen Sponsored Research Agreement to J.E.Y., a Retromer Therapeutic Sponsored Research Agreement to J.E.Y. and NIH traning grant (T32AG052354) to A.K. and a generous gift from the Ellison Foundation (to UW).

Author contributions Conceptualization: JEY, SM, and AK. Microscopy analysis: SM, AK, and DWH. RNA-seq analysis and bioinformatics: YW and AK. Methodology: SM, AK, MS, CAW, and CK. Writing—original draft: SM, AK and JEY. Writing—reviewing and editing: JEY, SM, and AK. Funding acquisition: JEY and AK. Supervision: JEY. All the authors read and approved the final manuscript.

Availability of data and material All raw and processed RNA-seq data have been deposited at the NCBI Gene Expression Omnibus (GSE180793). The data sets used and/or analyzed during the current study are available from the corresponding author on reasonable request.

Availability of supporting material All supporting data and material in the current study are available from the corresponding author on reasonable request.

Declarations

Conflict of interest The authors declare no competing interests.

Ethics approval and consent to participate Not applicable.

Consent for publication Not applicable.

Open Access This article is licensed under a Creative Commons Attribution 4.0 International License, which permits use, sharing, adaptation, distribution and reproduction in any medium or format, as long as you give appropriate credit to the original author(s) and the source, provide a link to the Creative Commons licence, and indicate if changes were made. The images or other third party material in this article are included in the article's Creative Commons licence, unless indicated otherwise in a credit line to the material. If material is not included in the article's Creative Commons licence and your intended use is not permitted by statutory regulation or exceeds the permitted use, you will need to obtain permission directly from the copyright holder. To view a copy of this licence, visit http://creativecommons.org/licenses/by/4.0/.

References

1. Al-Akhrass H, Conway JRW, Poulsen ASA, Paatero I, Kaivola J, Padzik A, Andersen OM, Ivaska J (2021) A feed-forward loop between SorLA and HER3 determines heregulin response and neratinib resistance. Oncogene 40:1300–1317
2. Alexa A, Rahnenfuhrer J, Lengauer T (2006) Improved scoring of functional groups from gene expression data by decorrelating GO graph structure. Bioinformatics 22:1600–1607
3. Anders S, Huber W (2010) Differential expression analysis for sequence count data. Genome Biol 11:R106
4. Andersen OM, Reiche J, Schmidt V, Gotthardt M, Spoelgen R, Behlke J, von Arnim CA, Breiderhoff T, Jansen P, Wu X et al (2005) Neuronal sorting protein-related receptor sorLA/LR11 regulates processing of the amyloid precursor protein. Proc Natl Acad Sci USA 102:13461–13466
5. Andersen OM, Bøgh N, Landau AM, Pløen GG, Jensen AMG, Monti G, Ulhøi BP, Nyengaard JR, Jacobsen KR, Jørgensen MM, Holm IE, Kristensen ML, Hansen ESS, Teunissen CE, Breidenbach L, Droescher M, Liu Y, Pedersen HS, Callesen H, Luo Y, Bolund L, Brooks DJ, Laustsen C, Small SA, Mikkelsen LF, Sørensen CB (2021) In vivo evidence that SORL1, encoding the endosomal recycling receptor SORLA, can function as a causal gene in Alzheimer's Disease. https://doi.org/10.1101/2021.07.13.452149
6. Bohm C, Seibel NM, Henkel B, Steiner H, Haass C, Hampe W (2006) SorLA signaling by regulated intramembrane proteolysis. J Biol Chem 281:14547–14553
7. Bolte S, Cordelieres FP (2006) A guided tour into subcellular colocalization analysis in light microscopy. J Microsc 224:213–232
8. Caglayan S, Takagi-Niidome S, Liao F, Carlo AS, Schmidt V, Burgert T, Kitago Y, Fuchtbauer EM, Fuchtbauer A, Holtzman DM et al (2014). Lysosomal sorting of amyloid-beta by the SORLA receptor is impaired by a familial Alzheimer's disease mutation. Science translational medicine 6:223ra220
9. Cataldo AM, Peterhoff CM, Troncoso JC, Gomez-Isla T, Hyman BT, Nixon RA (2000) Endocytic pathway abnormalities precede amyloid beta deposition in sporadic Alzheimer's disease and Down syndrome: differential effects of APOE genotype and presenilin mutations. Am J Pathol 157:277–286
10. Chambers SM, Fasano CA, Papapetrou EP, Tomishima M, Sadelain M, Studer L (2009) Highly efficient neural conversion of human ES and iPS cells by dual inhibition of SMAD signaling. Nat Biotechnol 27:275–280
11. Cheng X-T, Xie Y-X, Zhou B, Huang N, Farfel-Becker T, Sheng Z-H (2018) Characterization of LAMP1-labeled nondegradative lysosomal and endocytic compartments in neurons. J Cell Biol 217:3127–3139
12. Choi JH, Kaur G, Mazzella MJ, Morales-Corraliza J, Levy E, Mathews PM (2013) Early endosomal abnormalities and cholinergic neuron degeneration in amyloid-beta protein precursor transgenic mice. J Alzheimers Dis 34:691–700
13. Csardi GNT (2006) The igraph software package for complex network research. Int J Complex Syst 1695:1–9
14. Cullen PJ, Steinberg F (2018) To degrade or not to degrade: mechanisms and significance of endocytic recycling. Nat Rev Mol Cell Biol 19:679–696
15. Das U, Wang L, Ganguly A, Saikia JM, Wagner SL, Koo EH, Roy S (2016) Visualizing APP and BACE-1 approximation in neurons yields insight into the amyloidogenic pathway. Nat Neurosci 19:55–64
16. Davis SE, Roth JR, Aljabi Q, Hakim AR, Savell KE, Day JJ, Arrant AE (2021) Delivering progranulin to neuronal lysosomes protects against excitotoxicity. J Biol Chem 297:100993
17. de Araujo MEG, Liebscher G, Hess MW, Huber LA (2020) Lysosomal size matters. Traffic 21:60–75
18. Devi L, Ohno M (2015) TrkB reduction exacerbates Alzheimer's disease-like signaling aberrations and memory deficits without affecting β-amyloidosis in 5XFAD mice. Transl Psychiatry 5:e562–e562
19. Dewar D, Chalmers DT, Graham DI, McCulloch J (1991) Glutamate metabotropic and AMPA binding sites are reduced in Alzheimer's disease: an autoradiographic study of the hippocampus. Brain Res 553:58–64
20. Dobin A, Davis CA, Schlesinger F, Drenkow J, Zaleski C, Jha S, Batut P, Chaisson M, Gingeras TR (2013) STAR: ultrafast universal RNA-seq aligner. Bioinformatics 29:15–21
21. Dodson SE, Gearing M, Lippa CF, Montine TJ, Levey AI, Lah JJ (2006) LR11/SorLA expression is reduced in sporadic Alzheimer disease but not in familial Alzheimer disease. J Neuropathol Exp Neurol 65:866–872
22. Dumanis SB, Burgert T, Caglayan S, Fuchtbauer A, Fuchtbauer EM, Schmidt V, Willnow TE (2015) Distinct functions for anterograde and retrograde sorting of SORLA in amyloidogenic processes in the brain. J Neurosci Off J Soc Neurosci 35:12703–12713
23. Dunn KW, Kamocka MM, McDonald JH (2011) A practical guide to evaluating colocalization in biological microscopy. Am J Physiol Cell Physiol 300:C723–C742
24. Farfel-Becker T, Roney JC, Cheng XT, Li S, Cuddy SR, Sheng ZH (2019) Neuronal soma-derived degradative lysosomes are continuously delivered to distal axons to maintain local degradation capacity. Cell Rep 28:51-64.e54
25. Fjorback AW, Seaman M, Gustafsen C, Mehmedbasic A, Gokool S, Wu C, Militz D, Schmidt V, Madsen P, Nyengaard JR et al (2012) Retromer binds the FANSHY sorting motif in SorLA to regulate amyloid precursor protein sorting and processing. J Neurosci 32:1467–1480
26. Ginsberg, S.D., Malek-Ahmadi, M.H., Alldred, M.J., Chen, Y., Chen, K., Chao, M.V., Counts, S.E., and Mufson, E.J. (2019). Brain-derived neurotrophic factor (BDNF) and TrkB hippocampal gene expression are putative predictors of neuritic plaque and neurofibrillary tangle pathology. Neurobiology of Disease *132*, 104540.
27. Glerup S, Lume M, Olsen D, Nyengaard JR, Vaegter CB, Gustafsen C, Christensen EI, Kjolby M, Hay-Schmidt A, Bender D et al (2013) SorLA controls neurotrophic activity by sorting of GDNF and its receptors GFRalpha1 and RET. Cell Rep 3:186–199
28. Gowrishankar S, Yuan P, Wu Y, Schrag M, Paradise S, Grutzendler J, De Camilli P, Ferguson SM (2015) Massive accumulation of luminal protease-deficient axonal lysosomes at Alzheimer's disease amyloid plaques. Proc Natl Acad Sci 112:E3699–E3708
29. Grant BD, Donaldson JG (2009) Pathways and mechanisms of endocytic recycling. Nat Rev Mol Cell Biol 10:597–608
30. Hamasaki M, Araki N, Hatae T (2004) Association of early endosomal autoantigen 1 with macropinocytosis in EGF-stimulated A431 cells. Anat Rec A Discov Mol Cell Evol Biol 277:298–306
31. Herskowitz JH, Offe K, Deshpande A, Kahn RA, Levey AI, Lah JJ (2012) GGA1-mediated endocytic traffic of LR11/SorLA alters APP intracellular distribution and amyloid-beta production. Mol Biol Cell 23:2645–2657
32. Hojland A, Richner M, Molgaard S, Dieu RS, Eskelund A, Nykjaer A, Nyengaard JR, Lykkesfeldt J, Glerup S, Nielsen MS (2018) Biochemical and cognitive effects of docosahexaenoic acid differ in a developmental and SorLA dependent manner. Behav Brain Res 348:90–100
33. Holstege H, van der Lee SJ, Hulsman M, Wong TH, van Rooij JG, Weiss M, Louwersheimer E, Wolters FJ, Amin N, Uitterlinden AG et al (2017) Characterization of pathogenic SORL1 genetic

variants for association with Alzheimer's disease: a clinical interpretation strategy. Eur J Hum Genet 25:973–981

34. Huang TY, Zhao Y, Jiang LL, Li X, Liu Y, Sun Y, Pina-Crespo JC, Zhu B, Masliah E, Willnow TE et al (2017) SORLA attenuates EphA4 signaling and amyloid beta-induced neurodegeneration. J Exp Med 214:3669–3685
35. Huang TY, Zhao Y, Li X, Wang X, Tseng IC, Thompson R, Tu S, Willnow TE, Zhang YW, Xu H (2016) SNX27 and SORLA interact to reduce amyloidogenic subcellular distribution and processing of amyloid precursor protein. J Neurosci 36:7996–8011
36. Huang Z, Shimazu K, Woo NH, Zang K, Muller U, Lu B, Reichardt LF (2006) Distinct roles of the beta 1-class integrins at the developing and the mature hippocampal excitatory synapse. J Neurosci 26:11208–11219
37. Hung C, Tuck E, Stubbs V, van der Lee SJ, Aalfs C, van Spaendonk R, Scheltens P, Hardy J, Holstege H, Livesey FJ (2021) SORL1 deficiency in human excitatory neurons causes APP-dependent defects in the endolysosome-autophagy network. Cell Rep 35:109259
38. Hwang J, Estick CM, Ikonne US, Butler D, Pait MC, Elliott LH, Ruiz S, Smith K, Rentschler KM, Mundell C et al (2019) The role of lysosomes in a broad disease-modifying approach evaluated across transgenic mouse models of Alzheimer's disease and Parkinson's disease and models of mild cognitive impairment. Int J Mol Sci 20:4432
39. Jacobsen L, Madsen P, Nielsen MS, Geraerts WP, Gliemann J, Smit AB, Petersen CM (2002) The sorLA cytoplasmic domain interacts with GGA1 and -2 and defines minimum requirements for GGA binding. FEBS Lett 511:155–158
40. Karch CM, Goate AM (2015) Alzheimer's disease risk genes and mechanisms of disease pathogenesis. Biol Psychiatry 77:43–51
41. Klinger SC, Siupka P, Nielsen MS (2015) Retromer-mediated trafficking of transmembrane receptors and transporters. Membranes (Basel) 5:288–306
42. Knupp A, Mishra S, Martinez R, Braggin JE, Szabo M, Kinoshita C, Hailey DW, Small SA, Jayadev S, Young JE (2020) Depletion of the AD risk gene SORL1 selectively impairs neuronal endosomal traffic independent of amyloidogenic APP processing. Cell Rep 31:107719
43. Koopmans F, van Nierop P, Andres-Alonso M, Byrnes A, Cijsouw T, Coba MP, Cornelisse LN, Farrell RJ, Goldschmidt HL, Howrigan DP et al (2019) SynGO: an evidence-based, expert-curated knowledge base for the synapse. Neuron 103:217–234
44. Kwart D, Gregg A, Scheckel C, Murphy EA, Paquet D, Duffield M, Fak J, Olsen O, Darnell RB, Tessier-Lavigne M (2019) A large panel of isogenic APP and PSEN1 mutant human iPSC neurons reveals shared endosomal abnormalities mediated by APP beta-CTFs, not abeta. Neuron 104:256–270
45. Lambert JC, Ibrahim-Verbaas CA, Harold D, Naj AC, Sims R, Bellenguez C, Jun G, Destefano AL, Bis JC, Beecham GW et al (2013) Meta-analysis of 74,046 individuals identifies 11 new susceptibility loci for Alzheimer's disease. Nat Genet 45:1452–1458
46. Leek JT, Johnson WE, Parker HS, Jaffe AE, Storey JD (2012) The sva package for removing batch effects and other unwanted variation in high-throughput experiments. Bioinformatics 28:882–883
47. Levy S, Sutton G, Ng PC, Feuk L, Halpern AL, Walenz BP, Axelrod N, Huang J, Kirkness EF, Denisov G et al (2007) The diploid genome sequence of an individual human. PLoS Biol 5:e254
48. Li B, Dewey CN (2011) RSEM: accurate transcript quantification from RNA-Seq data with or without a reference genome. BMC Bioinform 12:323
49. Lorenzen A, Samosh J, Vandewark K, Anborgh PH, Seah C, Magalhaes AC, Cregan SP, Ferguson SSG, Pasternak SH (2010) Rapid and direct transport of cell surface APP to the lysosome defines a novel selective pathway. Mol Brain 3:11
50. Mallard F, Antony C, Tenza D, Salamero J, Goud B, Johannes L (1998) Direct pathway from early/recycling endosomes to the Golgi apparatus revealed through the study of shiga toxin B-fragment transport. J Cell Biol 143:973–990
51. Manders E, Verbeek F, Aten J (1993) Measurement of co-localization of objects in dual-colour confocal images. J Microsc 169:375–382
52. Marsh EW, Leopold PL, Jones NL, Maxfield FR (1995) Oligomerized transferrin receptors are selectively retained by a lumenal sorting signal in a long-lived endocytic recycling compartment. J Cell Biol 129:1509–1522
53. Martin-Belmonte A, Aguado C, Alfaro-Ruiz R, Itakura M, Moreno-Martinez AE, de la Ossa L, Molnar E, Fukazawa Y, Lujan R (2020) Age-Dependent shift of AMPA receptors from synapses to intracellular compartments in Alzheimer's disease: immunocytochemical analysis of the CA1 hippocampal region in APP/PS1 transgenic mouse model. Front Aging Neurosci 12:577996
54. Marwaha R, Sharma M (2017) DQ-Red BSA trafficking assay in cultured cells to assess cargo delivery to lysosomes. Bio Protoc 7:
55. Maxfield FR, McGraw TE (2004) Endocytic recycling. Nat Rev Mol Cell Biol 5:121–132
56. Mayle KM, Le AM, Kamei DT (2012) The intracellular trafficking pathway of transferrin. Biochim Biophys Acta 1820:264–281
57. McQuin C, Goodman A, Chernyshev V, Kamentsky L, Cimini BA, Karhohs KW, Doan M, Ding L, Rafelski SM, Thirstrup D et al (2018) Cell Profiler 3.0: next-generation image processing for biology. PLoS Biol 16:e2005970
58. Muller T, Meyer HE, Egensperger R, Marcus K (2008) The amyloid precursor protein intracellular domain (AICD) as modulator of gene expression, apoptosis, and cytoskeletal dynamics-relevance for Alzheimer's disease. Prog Neurobiol 85:393–406
59. Offe K, Dodson SE, Shoemaker JT, Fritz JJ, Gearing M, Levey AI, Lah JJ (2006) The lipoprotein receptor LR11 regulates amyloid beta production and amyloid precursor protein traffic in endosomal compartments. J Neurosci 26:1596–1603
60. Ouellette SP, Carabeo RA (2010) A functional slow recycling pathway of transferrin is required for growth of chlamydia. Front Microbiol 1:112
61. Park M, Penick EC, Edwards JG, Kauer JA, Ehlers MD (2004) Recycling endosomes supply AMPA receptors for LTP. Science 305:1972–1975
62. Patapoutian A, Reichardt LF (2001) Trk receptors: mediators of neurotrophin action. Curr Opin Neurobiol 11:272–280
63. Pietila M, Sahgal P, Peuhu E, Jantti NZ, Paatero I, Narva E, Al-Akhrass H, Lilja J, Georgiadou M, Andersen OM et al (2019) SORLA regulates endosomal trafficking and oncogenic fitness of HER2. Nat Commun 10:2340
64. Qureshi YH, Patel VM, Berman DE, Kothiya MJ, Neufeld JL, Vardarajan B, Tang M, Reyes-Dumeyer D, Lantigua R, Medrano M et al (2018) An Alzheimer's disease-linked loss-of-function CLN5 variant impairs cathepsin D maturation, consistent with a retromer trafficking defect. Mol Cell Biol 38:e00011–e00018
65. Racoosin EL, Swanson JA (1993) Macropinosome maturation and fusion with tubular lysosomes in macrophages. J Cell Biol 121:1011–1020
66. Raghavan NS, Brickman AM, Andrews H, Manly JJ, Schupf N, Lantigua R, Wolock CJ, Kamalakaran S, Petrovski S, Tosto G et al (2018) Whole-exome sequencing in 20,197 persons for rare variants in Alzheimer's disease. Ann Clin Transl Neurol 5:832–842
67. Ramilowski JA, Goldberg T, Harshbarger J, Kloppmann E, Lizio M, Satagopam VP, Itoh M, Kawaji H, Carninci P, Rost B et al (2015) A draft network of ligand-receptor-mediated multicellular signalling in human. Nat Commun 6:7866

68. Rapaport D, Lugassy Y, Sprecher E, Horowitz M (2010) Loss of SNAP29 impairs endocytic recycling and cell motility. PLoS ONE 5:e9759
69. Ren M, Xu G, Zeng J, De Lemos-Chiarandini C, Adesnik M, Sabatini DD (1998) Hydrolysis of GTP on rab11 is required for the direct delivery of transferrin from the pericentriolar recycling compartment to the cell surface but not from sorting endosomes. Proc Natl Acad Sci USA 95:6187–6192
70. Rogaeva E, Meng Y, Lee JH, Gu Y, Kawarai T, Zou F, Katayama T, Baldwin CT, Cheng R, Hasegawa H et al (2007) The neuronal sortilin-related receptor SORL1 is genetically associated with Alzheimer disease. Nat Genet 39:168–177
71. Rohe M, Hartl D, Fjorback AN, Klose J, Willnow TE (2013) SORLA-mediated trafficking of TrkB enhances the response of neurons to BDNF. PLoS ONE 8:e72164
72. Romano R, Rivellini C, De Luca M, Tonlorenzi R, Beli R, Manganelli F, Nolano M, Santoro L, Eskelinen E-L, Previtali SC et al (2021) Alteration of the late endocytic pathway in Charcot–Marie–Tooth type 2B disease. Cell Mol Life Sci 78:351–372
73. Scheltens P, De Strooper B, Kivipelto M, Holstege H, Chetelat G, Teunissen CE, Cummings J, van der Flier WM (2021) Alzheimer's disease. Lancet 397:1577–1590
74. Schindelin J, Arganda-Carreras I, Frise E, Kaynig V, Longair M, Pietzsch T, Preibisch S, Rueden C, Saalfeld S, Schmid B et al (2012) Fiji: an open-source platform for biological-image analysis. Nat Methods 9:676–682
75. Schmidt V, Sporbert A, Rohe M, Reimer T, Rehm A, Andersen OM, Willnow TE (2007) SorLA/LR11 regulates processing of amyloid precursor protein via interaction with adaptors GGA and PACS-1. J Biol Chem 282:32956–32964
76. Seaman MN (2004) Cargo-selective endosomal sorting for retrieval to the Golgi requires retromer. J Cell Biol 165:111–122
77. Seaman MN (2012) The retromer complex—endosomal protein recycling and beyond. J Cell Sci 125:4693–4702
78. Selkoe DJ (2002) Alzheimer's disease is a synaptic failure. Science 298:789–791
79. Shi Y, Kirwan P, Smith J, Robinson HP, Livesey FJ (2012) Human cerebral cortex development from pluripotent stem cells to functional excitatory synapses. Nat Neurosci 15:477–486, S471
80. Simoes S, Guo J, Buitrago L, Qureshi YH, Feng X, Kothiya M, Cortes E, Patel V, Kannan S, Kim YH et al (2021) Alzheimer's vulnerable brain region relies on a distinct retromer core dedicated to endosomal recycling. Cell Rep 37:110182
81. Simoes S, Neufeld JL, Triana-Baltzer G, Moughadam S, Chen EI, Kothiya M, Qureshi YH, Patel V, Honig LS, Kolb H et al (2020) Tau and other proteins found in Alzheimer's disease spinal fluid are linked to retromer-mediated endosomal traffic in mice and humans. Sci Transl Med 12:eaba6334
82. Simoes S, Guo J, Buitrago L, Qureshi YH, Feng X, Kothiya M, Cortes E, Patel V, Kannan S, Kim Y-H, Chang K-T, Hussaini A, Moreno H, Di Paolo G, Andersen OM, Small SA (2021) Alzheimer's vulnerable brain region relies on a distinct retromer core dedicated to endosomal recycling. Cell Rep 37:110182
83. Small SA, Gandy S (2006) Sorting through the cell biology of Alzheimer's disease: intracellular pathways to pathogenesis. Neuron 52:15–31
84. Small SA, Petsko GA (2020) Endosomal recycling reconciles the Alzheimer's disease paradox. Sci Transl Med 12:eabb1717
85. Sonnichsen B, De Renzis S, Nielsen E, Rietdorf J, Zerial M (2000) Distinct membrane domains on endosomes in the recycling pathway visualized by multicolor imaging of Rab4, Rab5, and Rab11. J Cell Biol 149:901–914
86. Spoelgen R, von Arnim CA, Thomas AV, Peltan ID, Koker M, Deng A, Irizarry MC, Andersen OM, Willnow TE, Hyman BT (2006) Interaction of the cytosolic domains of sorLA/LR11 with the amyloid precursor protein (APP) and beta-secretase beta-site APP-cleaving enzyme. J Neurosci 26:418–428
87. Sun J, Roy S (2018) The physical approximation of APP and BACE-1: a key event in alzheimer's disease pathogenesis. Dev Neurobiol 78:340–347
88. Temkin P, Morishita W, Goswami D, Arendt K, Chen L, Malenka R (2017) The retromer supports AMPA receptor trafficking during LTP. Neuron 94:74–82, e75
89. Thonberg H, Chiang HH, Lilius L, Forsell C, Lindstrom AK, Johansson C, Bjorkstrom J, Thordardottir S, Sleegers K, Van Broeckhoven C et al (2017) Identification and description of three families with familial Alzheimer disease that segregate variants in the SORL1 gene. Acta Neuropathol Commun 5:43
90. Tian X, Gala U, Zhang Y, Shang W, Nagarkar Jaiswal S, di Ronza A, Jaiswal M, Yamamoto S, Sandoval H, Duraine L et al (2015) A voltage-gated calcium channel regulates lysosomal fusion with endosomes and autophagosomes and is required for neuronal homeostasis. PLoS Biol 13:e1002103
91. Wakabayashi K, Narisawa-Saito M, Iwakura Y, Arai T, Ikeda K, Takahashi H, Nawa H (1999) Phenotypic down-regulation of glutamate receptor subunit GluR1 in Alzheimer's disease. Neurobiol Aging 20:287–295
92. Wang Y, Eng DG, Kaverina NV, Loretz CJ, Koirala A, Akilesh S, Pippin JW, Shankland SJ (2020) Global transcriptomic changes occur in aged mouse podocytes. Kidney Int 98:1160–1173
93. Willnow TE, Andersen OM (2013) Sorting receptor SORLA—a trafficking path to avoid Alzheimer disease. J Cell Sci 126:2751–2760
94. Yap CC, Digilio L, McMahon LP, Garcia ADR, Winckler B (2018) Degradation of dendritic cargos requires Rab7-dependent transport to somatic lysosomes. J Cell Biol 217:3141–3159
95. Yasuda RP, Ikonomovic MD, Sheffield R, Rubin RT, Wolfe BB, Armstrong DM (1995) Reduction of AMPA-selective glutamate receptor subunits in the entorhinal cortex of patients with Alzheimer's disease pathology: a biochemical study. Brain Res 678:161–167
96. Young JE, Boulanger-Weill J, Williams DA, Woodruff G, Buen F, Revilla AC, Herrera C, Israel MA, Yuan SH, Edland SD et al (2015) Elucidating molecular phenotypes caused by the SORL1 Alzheimer's disease genetic risk factor using human induced pluripotent stem cells. Cell Stem Cell 16:373–385
97. Yuan SH, Martin J, Elia J, Flippin J, Paramban RI, Hefferan MP, Vidal JG, Mu Y, Killian RL, Israel MA et al (2011) Cell-surface marker signatures for the isolation of neural stem cells, glia and neurons derived from human pluripotent stem cells. PLoS ONE 6:e17540
98. Zigdon H, Meshcheriakova A, Farfel-Becker T, Volpert G, Sabanay H, Futerman AH (2017) Altered lysosome distribution is an early neuropathological event in neurological forms of Gaucher disease. FEBS Lett 591:774–783

Publisher's Note Springer Nature remains neutral with regard to jurisdictional claims in published maps and institutional affiliations.

Authors and Affiliations

Swati Mishra[1,2] · **Allison Knupp**[1,2] · **Marcell P. Szabo**[1,2] · **Charles A. Williams**[1,2] · **Chizuru Kinoshita**[1,2] · **Dale W. Hailey**[1,2] · **Yuliang Wang**[2,3] · **Olav M. Andersen**[4] · **Jessica E. Young**[1,2]

Swati Mishra
swatim2@uw.edu

Allison Knupp
knuppa@uw.edu

Marcell P. Szabo
szabom@uw.edu

Charles A. Williams
cwil@uw.edu

Chizuru Kinoshita
ckino@uw.edu

Dale W. Hailey
dhailey@uw.edu

Yuliang Wang
yuliangw@uw.edu

Olav M. Andersen
o.andersen@biomed.au.dk

[1] Department of Laboratory Medicine and Pathology, University of Washington, Seattle, WA 98195, USA

[2] Institute for Stem Cell and Regenerative Medicine, University of Washington, Seattle, WA 98195, USA

[3] Paul G. Allen School of Computer Science and Engineering, University of Washington, Seattle, WA 98195, USA

[4] Department of Biomedicine, Danish Research Institute of Translational Neuroscience (DANDRITE), Aarhus University, Aarhus, Denmark